single nucleotide polymorphism (SNP) microarrays using genomic DNA extracted from the vitreous fluids.

Materials and Methods

Study design. The patients in this study were referred to the Tokyo Medical and Dental University (TMDU) or the Tokyo Medical University (TMU) hospital (both Tokyo, Japan) on suspicion of IOL between 2005 and 2011. After the diagnosis was made, they were treated at TMDU, TMU, or the primary hospitals from which they were referred.

The vitreous fluid of IOL patients was analyzed at TMDU, TMU, and The University of Tokyo (Tokyo, Japan). Patients who were HIV-positive were excluded. Written informed consent was obtained from patients except those who had already passed away. Obtaining the preserved samples with or without informed consent was approved by the ethics boards of these institutes.

Diagnosis and definition of IOL. Intraocular lymphoma was diagnosed using the following criteria: (i) typical eye involvement, a cloudy vitreous body and/or subretinal proliferative lesions; (ii) presence of lymphoma cells in the vitreous fluid; and (iii) clonality of the infiltrating lymphoma cells in the vitreous fluid using either PCR analysis of IgH or T-cell receptor gene rearrangements.[5] Patients who had criterion (i) accompanied by either (ii) or (iii) were diagnosed with IOL.[13]

In this report, IOL confined to the eyes at diagnosis was defined as PIOL. Intraocular lymphoma accompanied by central nervous system (CNS) lesions at diagnosis was defined as IOL with CNS lesion (IOCNSL). As it could not be determined whether the eyes or the CNS was the primary site, we analyzed IOCNSL independently from PIOL. Patients with IOL who developed ocular lesions after detection of lymphoma of extraocular and extra-CNS sites were categorized as having secondary IOL (SIOL). Pathological examination and investigation of systemic involvement were carried out at the

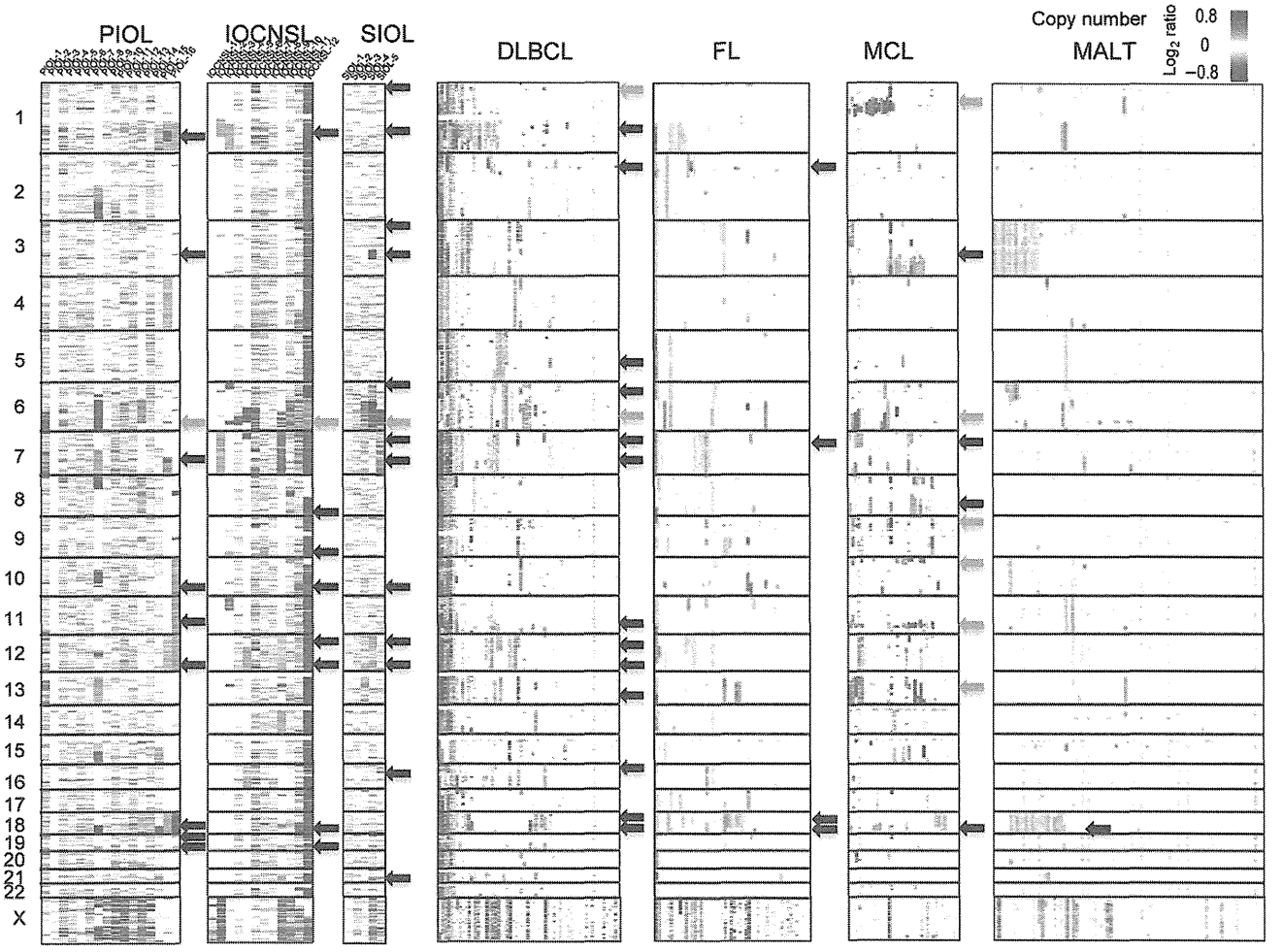

Fig. 1. Distributions of copy number (CN) changes in intraocular lymphomas (IOLs) and different lymphoma type samples. The latter includes data of 238 primary B-cell lymphomas, including 64 samples of diffuse large B-cell lymphomas (DLBCLs), 52 follicular lymphomas (FL), 35 mantle cell lymphomas (MCLs), and 87 mucosa-associated lymphoid tissue (MALT) lymphomas reported in Kato *et al.*[14] Genetic lesions are color-coded and plotted for each sample, as indicated. Samples were clustered in each lymphoma type. Regions with frequent CN change are indicated by arrows (black arrows, CN gains ≥50% in IOLs, ≥20% in the other lymphomas; orange arrows, CN losses). Note that genetic changes involving small regions are lost in this figure due to limited resolution. IOCNSL, IOL with a central nervous system lesion at diagnosis; PIOL, primary IOL; SIOL, secondary IOL.

institutes from which patients were referred. Diagnosis of IOL was made at TMDU and TMU.

Measurement of intravitreal IL-10. To determine the concentrations of IL-6 or IL-10 in the vitreous fluids, 50 μL vitreous supernatant from each patient was applied for ELISA according to the manufacturer's instructions (Invitrogen, Camarillo, CA, USA). The lowest detection limits of the cytokines were 2.0 pg/mL for IL-6, and 1.0 pg/mL for IL-10.

Single nucleotide polymorphism microarray. Genomic DNA extracted from the vitreous fluid at the time of diagnosis was subjected to SNP array karyotyping using GeneChip 250K SNP arrays (Affymetrix, Santa Clara, CA, USA) as previously described.[14] Details of the procedures are described in Data S1.

Statistical analysis. For statistical analyses, the Mann–Whitney *U*-test was carried out using GraphPad Prism 5 (GraphPad Software, La Jolla, CA, USA).

Results

Patients. Thirty-three IOLs were analyzed, including 16 PIOLs, 12 IOCNSLs, and five SIOLs. Their clinical information and laboratory findings of the vitreous fluids are summarized in Tables 1 and S1, respectively.

Characteristics of the copy number changes of IOLs. Copy number (CN) changes of all IOL samples are shown in Figures 1 and 2. As in our previous report, we defined CN changes as CN gains, losses, as well as neutral loss of heterozygosity involving >3 Mb segments (Fig. 2). As shown in Figures 1 and 2(a), the most frequent CN gain region in PIOL was 1q, detected in 81% (13/16) of cases, followed by 18q and 19q in 69% (11/16), 12q in 63% (10/16), 7q and 11q in 56% (9/16), and 3q, 10q, and 19p in 50% (8/16). As shown in Figures 1 and 2(b,c), the most frequent CN loss in PIOLs was on 6q (44%, 7/16), whereas uniparental disomy was detected on various regions in only patient.

Previously we investigated CN changes of genes in 238 primary B-cell lymphoma specimens of different histological types, including 64 samples of DLBCLs, 52 follicular lymphomas (FL), 35 mantle cell lymphomas (MCLs), and 87 mucosa-associated lymphoid tissue (MALT) lymphomas.[14] The results of the present study were presented in comparison with them (Fig. 1). The most frequent CN gain region in DLBCL was 1q (>40%), and other frequent CN gains in DLBCL were found on 12q, 18q (>30%), and on 2p, 5q, 6p, 7p, 7q, 11q, 12p, 13q, 16p, and 18p (>20%), whereas CN losses were on 1p and on 6q (>20%). As shown in Figures 1 and 2, 56% (5/9) of the CN gains found in >50% of PIOLs were also detected in >20% of DLBCLs, and were the most frequent gains. Conversely, the three most frequent gains found in DLBCL (>30%; 1q, 12q, and 18q) were detected in >63% of PIOLs (Figs. 1,2a). In addition, the most frequent CN loss in PIOL was located on 6q, as in DLBCL (Fig. 2b). In

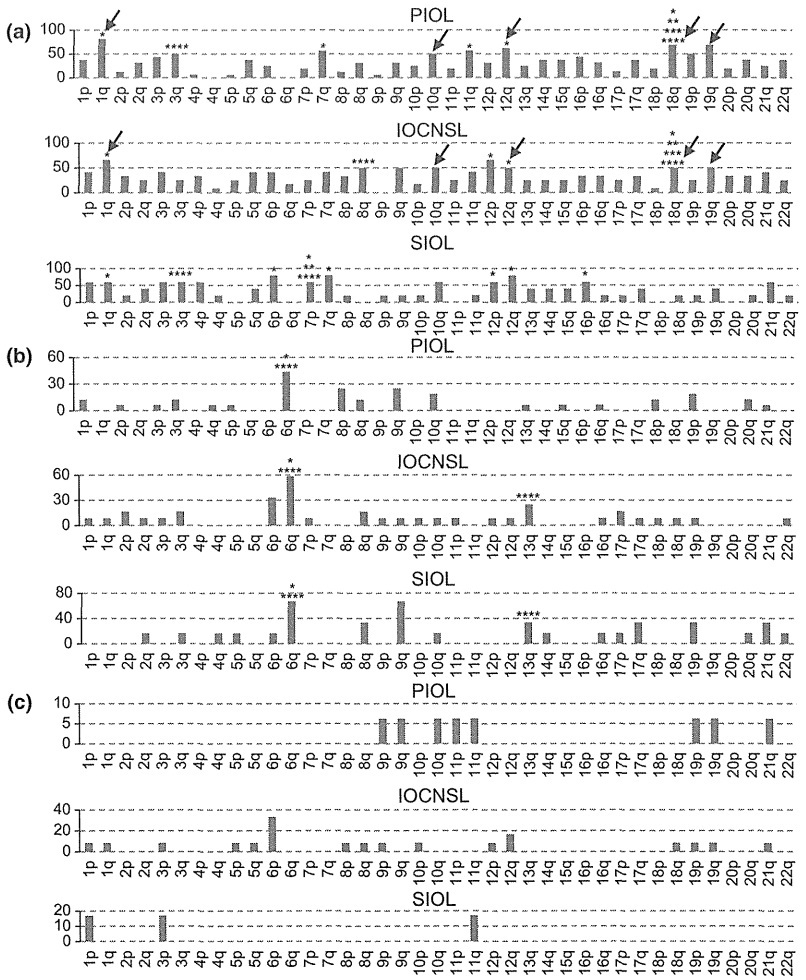

Fig. 2. Copy number (CN) change is summarized in each type of intraocular lymphoma (IOL). Frequency of CN gains (a) and losses (b), as well as CN neutral loss of heterozygosity (c) involving >3 Mb segments were calculated and plotted for each IOL type. *Copy number changes detected in >20% of diffuse large B-cell lymphomas; **CN changes detected in >20% of follicular lymphomas; ***CN changes detected in >20% of mucosa-associated lymphoid tissue lymphomas; ****CN changes detected in >20% of mantle cell lymphomas. Black arrows indicate common frequent (>50%) gain regions in primary IOL (PIOL), and in IOL with a central nervous system lesion at diagnosis (IOCNSL). SIOL, secondary IOL.

contrast, CN gains on 1q, which were the most frequent gains in PIOLs, were found infrequently (<10%) in FL, MALT lymphomas, and MCL.[14] Among the nine most frequent gains in PIOLs (≥50%), only CN gains on18q were frequent in FL or MALT lymphomas (>20%), and only two gains, on 3q and on 18q, were frequent in MCL (>30%) (Fig. 2a).

The most frequent CN gains in IOCNSLs were on 1q and 12p in 67% (8/12), followed by 8q, 9q, 10q, 12q, 18q, and 19q (6/12; 50%) (Fig. 2a). In SIOLs, frequent gains (≥50%) were detected on 13 chromosomal lesions (Fig. 2a). Among them, 50% (4/8) of gains in IOCNSLs and 55% (7/13) of gains in SIOLs were identical to those in DLBCL (>20%) (Fig. 2a). Frequent CN losses were located on the 6q region in IOCNSLs and SIOLs, (58% and 80%, respectively) (Fig. 2b).

Comparison between CN changes of IOLs. Next, we compared the genomic distribution of CN changes in each type of IOL. As shown in Figure 2(a), among the nine most frequent (≥50%) gain regions in PIOLs, five (5/9; 56%) regions (1q, 10q, 12q, 18q, and 19q) were also frequent (≥50%) in IOCNSLs. The most frequent gain in PIOL (13/16; 81%) was located on 1q, which was also the most frequent gain (8/12; 67%) in IOCNSLs (Fig. 2a). Concerning CN loss, 6q was the most frequent loss in PIOLs (7/16; 44%) and was also the most frequent (7/12; 58%) loss in IOCNSLs (Fig. 2a). These data indicated that PIOL and IOCNSL had common frequent CN alterations.

Some genes that affect the prognosis of lymphoma have already been described. It has been reported that PCNSL with deletion of 6q22.33, which contains *PTPRK*, revealed an aggressive clinical course.[15] As shown in Figure 3(a,b), loss of 6q22.33 was detected in 50% (6/12) of IOCNSLs and in 25% (4/16) of PIOLs. In addition, loss of 9p21.3, which contains *CDKN2A* (*p16*), was detected in 6/12 (50%) IOCNSLs (Fig. 3c), whereas it was deleted in 4/16 (25%) PIOLs (Fig. 3d). Among them, homozygous deletion of *CDKN2A* had occurred in two IOCNSL patients (Fig. 3e,f). Although statistical difference was not identified between them, loss of 6q22.33 and loss of 9p21.3 in IOCNSL seemed to be more common than that in PIOL.

Relation between genetic lesions and outcomes. The outcome of each patient is described in Table 1. Survival of patients with PIOL and IOCNSL is shown in Figure S1. The median overall survival (OS) of patients with PIOL was 37 months, whereas the OS of patients with IOCNSL and SIOL could not be determined due to the limited number of patients. Differences in OS between PIOL and IOCNSL patients could also not be evaluated due to the small number of patients.

Among 16 patients with PIOL, outcome could be followed in 12. As shown in Figure S2, four patients (PIOL-1, 10, 12, and 14) who had early CNS development within 6 months of the time of diagnosis had large CN loss lesions in 6q. Among them, three patients (PIOL-1, 10, and 12) had deletion of 6q22.33. In contrast, four patients (PIOL-6, 8, 13, and 16) who were alive without progression for more than 36 months did not have large deletions in 6q. We could not find a relation between loss of 9p21.3, which was detected in four patients (PIOL-11, 13, 14, and 15), and outcome.

High-grade amplifications or homozygous deletions. We identified several high-grade amplifications (Fig. 4). High-grade amplifications on eight lesions were found in PIOL-7 (Fig. 4a–e), whereas they were found on three lesions in PIOL-15 (Fig. 4f–h). High-grade amplification of 3p24.1-p23 was found in IOCNSL-11 (Fig. 4i). They were not recurrent in our case series. The genes in the affected regions are shown in Figure 4.

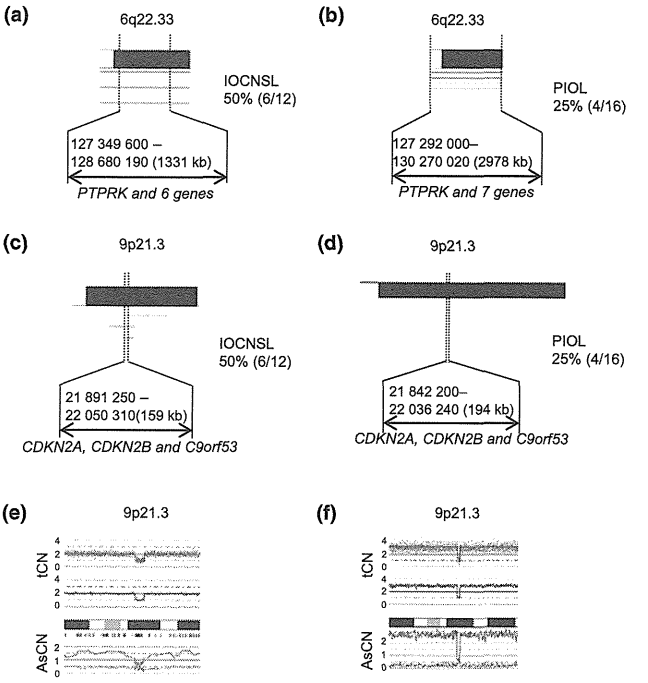

Fig. 3. Outputs of deletions of 6q22.33 and 9p21.3 in each type of intraocular lymphoma (IOL), generated by CNAG software. The CNAG software is freely available (http://www.genome.umin.jp/). (a) Chromosome 6q22.33 shows recurrent copy number (CN) loss in IOL with a central nervous system lesion at diagnosis (IOCNSL). The frequency in IOCNSL was 50% (6/12). (b) Chromosome 6q22.33 shows recurrent CN loss in primary IOL (PIOL). The frequency in PIOL was 25% (4/16). (c) Chromosome 9p21.3 shows recurrent CN loss in IOCNSL. The frequency in IOCNSL was 50% (6/12). (d) Chromosome 9p21.3 shows recurrent CN loss in PIOL. The frequency in PIOL was 25% (4/16). In figure parts (a–d), each horizontal line represents a CN loss found in a single case. (e,f) CNAG outputs of homozygous deletions of 9p21.3 in IOCNSL-9 (e) and IOCNSL-12 (f). Presence of homozygous deletions is indicated by the biallelic reduction of allele-specific CN (AsCN). tCN, total CN.

Copy number gain of *IL-10* gene and its concentration in vitreous fluid. The most frequent gain regions of PIOLs and IOCNSLs were located on 1q. It is noteworthy that the 1q32.1 region located on 1q contained the genes for *IL-10*, a cytokine whose concentration in the vitreous fluid is significantly high in IOL. The CN of the *IL-10* gene located on 1q32.1 was increased in 69% (11/16) of PIOLs, in 58% (7/12) of IOCNSL, in 80% (4/5) of SIOLs, and in 67% (22/33) in total. In order to examine the relation between CN change and IL-10 concentration, we compared the intravitreal IL-10 concentration of *IL-10* gain-positive patients to that of *IL-10* gain-negative patients. As shown in Figure 5(a), the IL-10 concentration of the gain-positive patients was significantly higher than that of the gain-negative patients in all IOLs. However, we could not find a significant difference between them in each IOL subtype (Fig. 5b,c), probably due to the small number of samples.

Discussion

Primary intraocular lymphoma consists of various histological types, but the majority are DLBCL. Our results showed that PIOLs diagnosed by analyzing the vitreous fluid and DLBCL

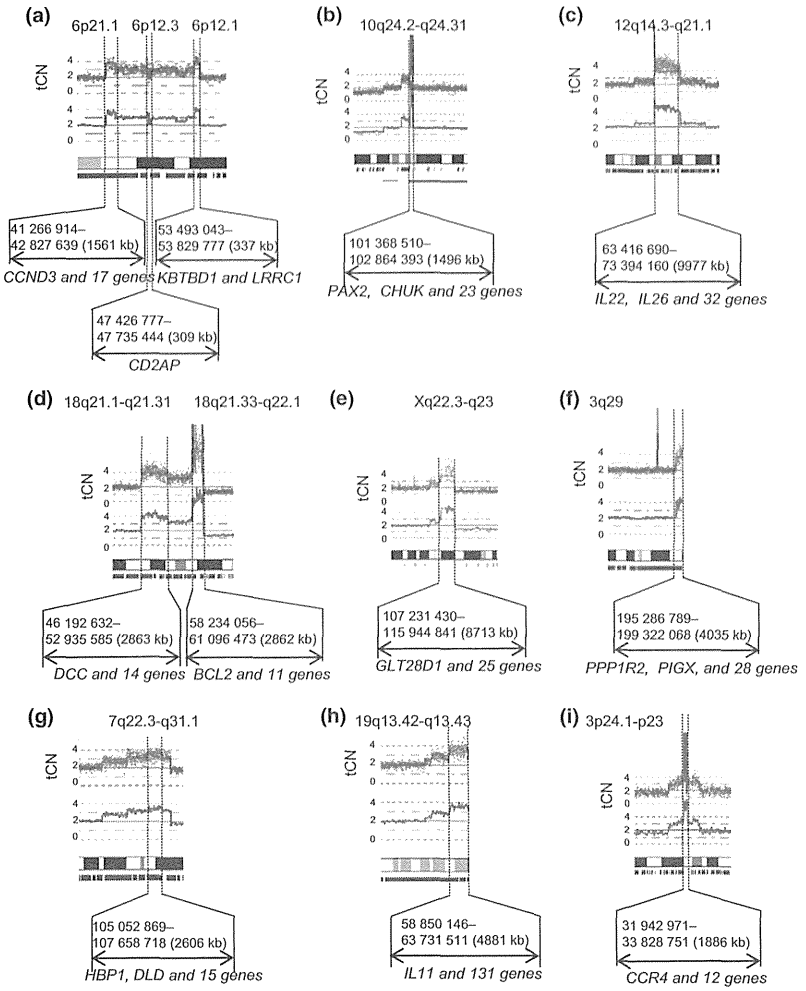

Fig. 4. Results of copy number analysis and outputs of high-grade amplifications in individual cases of intraocular lymphoma (IOL), generated by CNAG software. (a–e) Primary IOL (PIOL)-7. (f–h) PIOL-15. (i) IOL with a central nervous system lesion at diagnosis (IOCNSL)-11. Blue lines in the middle of each panel show the moving average of total copy numbers in five adjacent single nucleotide polymorphisms. The sample ID and possible gene targets are indicated in each panel.

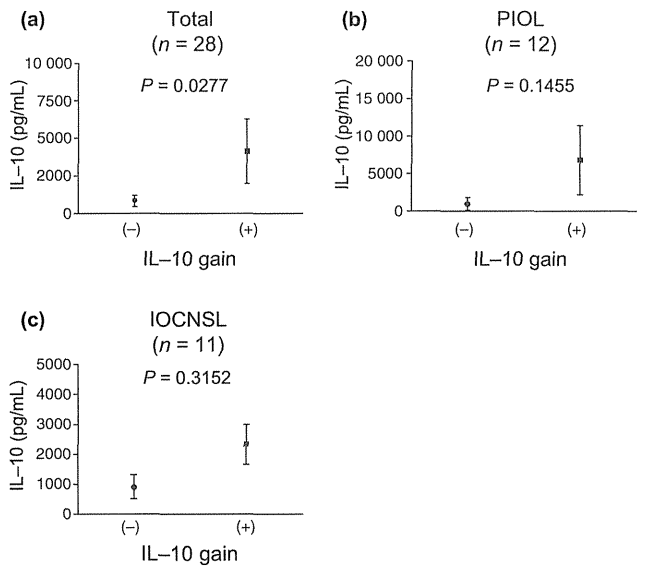

Fig. 5. Intravitreal interleukin-10 (IL-10) levels in intraocular lymphomas (IOLs) with or without gain of the *IL-10* gene. Data were analyzed for all patients (a), for primary IOL (PIOL) (b), and for IOL with a central nervous system lesion at diagnosis (IOCNSL) (c). The data represent the mean ± standard error of the mean.

had common CN-altered regions in their chromosomes. Therefore, it is appropriate to plan treatment for PIOL as an aggressive lymphoma.

The most frequent CN gain found in PIOLs was located on 1q that contained the region for the *IL-10* gene. Interestingly, there was correlation between gain of the *IL-10* gene and intravitreal IL-10 concentration. The concentration of IL-10 in the vitreous fluid is significantly higher in IOL than that in benign uveitis, and is a useful tool to distinguish between the two conditions.[5] In addition, IL-10 is an autocrine growth factor for B cells and promotes B-cell lymphoma development and proliferation.[16,17] Our results indicated that IL-10 may be secreted by the tumor cells and promote disease progression.

In the present report, loss of 6q22.33 was detected in 25% of PIOLs and 50% of IOCNSLs. According to previously published reports, the frequencies of del(6)(q22) in PCNSLs was 45%,[15] whereas that in systemic DLBCL was 25%.[18] Loss of 6q22.33 might be common in IOCNSL as in PCNSL compared to PIOL or systemic DLBCL. 6q22.33 contains *PTPRK*. This gene encodes protein tyrosine phosphatase receptor κ (PTPRK), which belongs to the protein tyrosine phosphatase superfamily of enzymes and inhibits proliferation- or survival-promoting molecular signals mediated by tyrosine kinase. It can act as a tumor suppressor by inhibiting cell cycle progression. It was reported that deletion of 6q22 in PCNSL revealed

an aggressive clinical course or poor prognosis.[15,19] Interestingly, three of four patients who had early CNS development and short survival periods had large CN loss in 6q, whereas long-term survivors did not have such deletions. Statistical analysis could not be carried out because of the limited number of patients. Further investigation should be undertaken to clarify the relation between deletion of 6q and outcome, especially the role of 6q22.33.

In our study, 9p21.3, on which *CDKN2A* was located, was deleted in 25% of PIOLs and 50% of IOCNSLs. Although statistical difference was not determined between them, loss of 9p21.3 might be more common in IOCNSL than in PIOL. *CDKN2A*, located in the other frequent loss region in IOCNSL, 9p21.3, negatively regulates G_1/S phase transition by inhibiting the kinase activity of CDK4/6. Thus, loss or inhibition of *CDKN2A* (*p16*) may result in increased tumor cell proliferation. In addition, it is well established that deletion of *CDKN2A* in DLBCL is associated with poor prognosis.[18] These findings suggested that IOCNSL was a highly malignant form of PIOL that tends to spread into the CNS at an early stage. Further clinical survey on a large scale should be added to confirm the hypothesis.

Although we have clarified some issues about the genetic characteristics of IOL, the origin of PIOL cells remains unknown. Wallace *et al.* detected t(14;18) in 67% of PIOL.[20] The high frequency of the translocation in PIOL suggests that the lymphoma cells originate from germinal center B-cells (GCBs) with high expression of BCL2.[21] Consistent with this, we found that the *BCL2* CN was increased in PIOL. The origin of PIOL cells, however, remains controversial. Lipford *et al.* reported that t(14;18) was determined in only 20% of PCNSL.[22] Other investigators indicated a high somatic mutation load in the VH genes of PIOL cells.[23] Furthermore, the immunophenotype of the PIOL tumor cells is MUM1/IRF4$^+$; BCL-6$^{+/-}$;CD10$^-$. These results suggested that PIOL was an activated B-cell subtype of DLBCL.[24] Further studies, including gene expression profiling, are required to confirm these results and to identify the cell of origin in PIOL lesions.

It has been reported that PIOL and PCNSL were closely related with each other. The majority of PIOL and PCNSL cases are pathologically diagnosed as DLBCL, and 60–82.5% of PIOL patients ultimately develop CNS lesions, whereas extra-CNS lesions are rare.[6,11,25,26] In addition, the eyes are close to the CNS and are actually derived from the CNS during embryogenesis. For these reasons, PIOL and PCNSL are categorized as the same lymphoma in many reports,[10,11] despite little genetic evidence to support this. As a result, potential differences between PIOL and PCNSL in their clinical features have not been evaluated. Our unpublished data, however, indicate that only one of 15 PCNSL patients diagnosed and treated during the last 10 years at our hospital developed eye lesions (Ayako Arai, unpublished data, 2013). In addition, the gain in chromosome 18, which was frequently detected in our PIOL series, was not described in the report by Sung and colleagues, the latest report for PCNSL analyzed by high-resolution array-based comparative genomic hybridization.[27] These findings suggest that PIOL and PCNSL may have distinct clinical courses and genetic features. Contrary to the report by Sung *et al.*, however, chromosome 18 was frequently gained in three early PCNSL reports.[28–30] The CN alteration in PCNSL has been controversial. The difference in methods may be one of the reasons for the discrepancies, and further study on the same technology platform should be carried out in order to determine the relation between PIOL and PCNSL.

Taken together, our data suggest that IOCNSL is considered to be a highly malignant form of PIOL that infiltrates into the CNS at an early stage. Study should be continued to clarify the the origin of tumor cells of PIOL, genetic alteration predicting outcome, and the genetic similarity and difference between PIOL and other B-cell lymphomas.

Acknowledgments

We are grateful to Ms. Kaori Okada for excellent technical assistance. This work was supported by grants from the Ministry of Education, Culture, Sports, Science, and Technology of Japan (23591375) and Japan Leukemia Research Fund.

Disclosure Statement

The authors have no conflict of interest.

References

1 Bardenstein DS. Intraocular lymphoma. *Cancer Control* 1998; **5**: 317–25.
2 Choi JY, Kafkala C, Foster CS. Primary intraocular lymphoma: a review. *Semin Ophthalmol* 2006; **21**: 125–33.
3 Coupland SE, Heimann H, Bechrakis NE. Primary intraocular lymphoma: a review of the clinical, histopathological and molecular biological features. *Graefes Arch Clin Exp Ophthalmol* 2004; **242**: 901–13.
4 Cassoux N, Merle-Beral H, Leblond V *et al.* Ocular and central nervous system lymphoma: clinical features and diagnosis. *Ocul Immunol Inflamm* 2000; **8**: 243–50.
5 Sugita S, Takase H, Sugamoto Y, Arai A, Miura O, Mochizuki M. Diagnosis of intraocular lymphoma by polymerase chain reaction analysis and cytokine profiling of the vitreous fluid. *Jpn J Ophthalmol* 2009; **53**: 209–14.
6 Kimura K, Usui Y, Goto H, Japanese Intraocular Lymphoma Study Group. Clinical features and diagnostic significance of the intraocular fluid of 217 patients with intraocular lymphoma. *Jpn J Ophthalmol* 2012; **56**: 383–9.
7 Shen DF, Zhuang Z, LeHoang P *et al.* Utility of microdissection and polymerase chain reaction for the detection of immunoglobulin gene rearrangement and translocation in primary intraocular lymphoma. *Ophthalmology* 1998; **105**: 1664–9.
8 Chan CC, Whitcup SM, Solomon D, Nussenblatt RB. Interleukin-10 in the vitreous of patients with primary intraocular lymphoma. *Am J Ophthalmol* 1995; **120**: 671–3.
9 Whitcup SM, Stark-Vancs V, Wittes RE *et al.* Association of interleukin 10 in the vitreous and cerebrospinal fluid and primary central nervous system lymphoma. *Arch Ophthalmol* 1997; **115**: 1157–60.
10 Kluin PM, Deckert M, Ferry JA. Primary diffuse large B-cell lymphoma of the CNS. In: Jaffe E, Harris N, Stein H, eds. *World Health Organization Classification of Tumors Pathology and Genetics of Tumours of Haematopoietic and Lymphoid Tissues*. Lyon: IARC Press, 2008; 240–1.
11 Coupland SE, Chan CC, Smith J. Pathophysiology of retinal lymphoma. *Ocul Immunol Inflamm* 2009; **17**: 227–37.
12 Chan CC, Sen HN. Current concepts in diagnosing and managing primary vitreoretinal (intraocular) lymphoma. *Discov Med* 2013; **15**: 93–100.
13 Nakauchi Y, Takase H, Sugita S *et al.* Concurrent administration of intravenous systemic and intravitreal methotrexate for intraocular lymphoma with central nervous system involvement. *Int J Hematol* 2010; **92**: 179–85.
14 Kato M, Sanada M, Kato I *et al.* Frequent inactivation of A20 in B-cell lymphomas. *Nature* 2009; **459**: 712–6.
15 Cady FM, O'Neill BP, Law ME *et al.* Del(6)(q22) and BCL6 rearrangements in primary CNS lymphoma are indicators of an aggressive clinical course. *J Clin Oncol* 2008; **26**: 4814–9.
16 Beatty PR, Krams SM, Martinez OM. Involvement of IL-10 in the autonomous growth of EBV-transformed B cell lines. *J Immunol* 1997; **158**: 4045–51.
17 Moore KW, de Waal Malefyt R, Coffman RL, O'Garra A Interleukin-10 and the interleukin-10 receptor. *Annu Rev Immunol.* 2001; **19**: 683–765.

18 Jardin F, Jais JP, Molina TJ *et al.* Diffuse large B-cell lymphomas with CDKN2A deletion have a distinct gene expression signature and a poor prognosis under R-CHOP treatment: a GELA study. *Blood* 2010; **116**: 1092–104.
19 Nakamura M, Kishi M, Sakaki T *et al.* Novel tumor suppressor loci on 6q22-23 in primary central nervous system lymphomas. *Cancer Res* 2003; **63**: 737–41.
20 Wallace DJ, Shen D, Reed GF *et al.* Detection of the bcl-2 t(14;18) translocation and proto-oncogene expression in primary intraocular lymphoma. *Invest Ophthalmol Vis Sci* 2006; **47**: 2750–6.
21 Alizadeh AA, Eisen MB, Davis RE *et al.* Distinct types of diffuse large B-cell lymphoma identified by gene expression profiling. *Nature* 2000; **403**: 503–11.
22 Lipford E, Wright JJ, Urba W *et al.* Refinement of lymphoma cytogenetics by the chromosome 18q21 major breakpoint region. *Blood* 1987; **70**: 1816–23.
23 Coupland SE, Hummel M, Müller HH, Stein H. Molecular analysis of immunoglobulin genes in primary intraocular lymphoma. *Invest Ophthalmol Vis Sci* 2005; **46**: 3507–14.
24 Coupland SE, Loddenkemper C, Smith JR *et al.* Expression of immunoglobulin transcription factors in primary intraocular lymphoma and primary central nervous system lymphoma. *Invest Ophthalmol Vis Sci* 2005; **46**: 3957–64.
25 Chan CC. Molecular pathology of primary intraocular lymphoma. *Trans Am Ophthalmol Soc* 2003; **101**: 275–92.
26 Coupland SE, Damato B. Understanding intraocular lymphomas. *Clin Experiment Ophthalmol* 2008; **36**: 564–78.
27 Sung CO, Kim SC, Karnan S *et al.* Genomic profiling combined with gene expression profiling in primary central nervous system lymphoma. *Blood* 2011; **117**: 1291–300.
28 Boonstra R, Koning A, Mastik M, van den Berg A, Poppema S. Analysis of chromosomal copy number changes and oncoprotein expression in primary central nervous system lymphomas: frequent loss of chromosome arm 6q. *Virchows Arch* 2003; **443**: 164–9.
29 Booman M, Szuhai K, Rosenwald A *et al.* Genomic alterations and gene expression in primary diffuse large B-cell lymphomas of immune-privileged sites: the importance of apoptosis and immunomodulatory pathways. *J Pathol* 2008; **216**: 209–17.
30 Harada K, Nishizaki T, Kubota H, Suzuki M, Sasaki K. Distinct primary central nervous system lymphoma defined by comparative genomic hybridization and laser scanning cytometry. *Cancer Genet Cytogenet* 2001; **125**: 147–50.

Supporting Information

Additional supporting information may be found in the online version of this article:

Fig. S1. Survival of patients with intraocular lymphoma (IOL). Differences in overall survival between patients with primary IOL (PIOL) and those with IOL with a central nervous system lesion at diagnosis (IOCNSL) could not be evaluated due to the small number of patients.

Fig. S2. Copy number alterations on chromosome 6 in primary intraocular lymphoma.

Table S1. Laboratory findings of the vitreous fluids of patients with intraocular lymphoma.

Appendix S1. Procedures of single nucleotide polymorphism microarray.

Published OnlineFirst March 27, 2014; DOI: 10.1158/0008-5472.CAN-13-2470

Molecular and Cellular Pathobiology

Cancer Research

Biallelic *DICER1* Mutations in Sporadic Pleuropulmonary Blastoma

Masafumi Seki[1], Kenichi Yoshida[2,6], Yuichi Shiraishi[3], Teppei Shimamura[3], Yusuke Sato[2,6], Riki Nishimura[1], Yusuke Okuno[2], Kenichi Chiba[3], Hiroko Tanaka[4], Keisuke Kato[7], Motohiro Kato[1,5,8], Ryoji Hanada[5], Yuko Nomura[9], Myoung-Ja Park[10], Toshiaki Ishida[11], Akira Oka[1], Takashi Igarashi[1,12], Satoru Miyano[3,4], Yasuhide Hayashi[9], Seishi Ogawa[2,6], and Junko Takita[1]

Abstract

Pleuropulmonary blastoma (PPB) is a rare pediatric malignancy whose pathogens are poorly understood. Recent reports suggest that germline mutations in the microRNA-processing enzyme DICER1 may contribute to PPB development. To investigate the genetic basis of this cancer, we performed whole-exome sequencing or targeted deep sequencing of multiple cases of PPB. We found biallelic *DICER1* mutations to be very common, more common than *TP53* mutations also found in many tumors. Somatic ribonuclease III (RNase IIIb) domain mutations were identified in all evaluable cases, either in the presence or absence of nonsense/frameshift mutations. Most cases had mutated *DICER1* alleles in the germline with or without an additional somatic mutation in the remaining allele, whereas other cases displayed somatic mutations exclusively where the RNase IIIb domain was invariably affected. Our results highlight the role of RNase IIIb domain mutations in *DICER1* along with TP53 inactivation in PPB pathogenesis. *Cancer Res; 74(10); 2742–9. ©2014 AACR.*

Introduction

Pleuropulmonary blastoma (PPB) is an extremely rare and highly aggressive pulmonary malignancy occurring in early childhood. It is characterized histologically by a primitive blastoma and a malignant mesenchymal stroma in the lung that often shows multidirectional differentiation (1). PPB may be sporadic or hereditary and may also present as a part of a familial tumor syndrome (2) consisting of cystic nephroma and other tumor types, such as ovarian tumor, embryonal rhabdomyosarcoma, and malignant germ cell tumors (2). Recently, germline *DICER1* mutations have been demonstrated in majority of patients with PPB and DICER1 syndrome (2, 3). *DICER1* is a member of the ribonuclease III (RNase III) protein family that is involved in the generation of microRNAs (miRNA), modulating gene expression at the posttranscriptional level (4). The DICER1 protein contains RNase IIIa and RNase IIIb domains, which are considered to dimerize intramolecularly with Mg^{2+}/Mn^{2+} to form the active site of the enzyme (5). In PPB, almost all mutations are reported to be heterozygous frameshift or nonsense mutations of germline origin, suggesting an important role of *DICER1* haploinsufficiency in PPB pathogenesis (2, 3). However, most obligate carriers of *DICER1* mutations and heterozygous *Dicer1*-deficient mice did not develop PPB or other types of tumors, suggesting that *DICER1* haploinsufficiency alone is insufficient for tumor development but requires additional genetic alterations (3, 6). To identify a complete set of genetic alterations underlying PPB pathogenesis, we performed whole-exome sequencing of paired tumor and normal DNA from seven cases with sporadic PPB, of which two cases were analyzed for samples obtained at both initial presentation and relapse. Mutations in *DICER1* and other genes were examined by targeted deep sequencing in 16 samples from 12 sporadic PPB cases, including three analyzed by whole-exome sequencing.

Materials and Methods

Specimens

Genomic DNA for 11 cases was extracted from fresh-frozen samples stored at −80 °C and obtained approximately 2 to 15 years previously. Paraffin-embedded samples were used as tumor samples for cases 10 (at relapse) and 11 (at diagnosis). These samples were stored for approximately 1 year. For

Authors' Affiliations: [1]Department of Pediatrics; [2]Cancer Genomics Project, Graduate School of Medicine; Laboratory of [3]DNA Information Analysis and [4]Sequence Data Analysis, Human Genome Center, Institute of Medical Science; [5]Department of Cell Therapy and Transplantation Medicine, The University of Tokyo, Tokyo; [6]Department of Pathology and Tumor Biology, Graduate School of Medicine, Kyoto University, Kyoto; [7]Division of Pediatric Hematology and Oncology, Ibaraki Children's Hospital, Mito, Ibaraki; [8]Department of Hematology/Oncology, Saitama Children's Medical Center, Saitama, Saitama; [9]Department of Pediatrics, School of Medicine, Fukuoka University, Fukuoka; [10]Gunma Children's Medical Center, Shibukawa, Gunma; [11]Department of Hematology and Oncology, Hyogo Prefectural Kobe Children's Hospital, Kobe, Hyogo; and [12]National Center for Child Health and Development, Tokyo, Japan

Note: Supplementary data for this article are available at Cancer Research Online (http://cancerres.aacrjournals.org/).

Corresponding Authors: Junko Takita, Department of Pediatrics, The University of Tokyo, 7-3-1 Hongo, Bunkyo-ku, Tokyo 113-8655, Japan. Phone: 81-3-3815-5411; Fax: 81-3-3816-4108; E-mail: jtakita-tky@umin.ac.jp; and Seishi Ogawa, Department of Pathology and Tumor Biology, Graduate School of Medicine, Kyoto University, Yoshida-Konoe-cho, Sakyo-ku, Kyoto 606-8501, Japan. Phone: 81-75-753-4300; Fax: 81-75-753-9282; E-mail: sogawa-tky@umin.ac.jp

doi: 10.1158/0008-5472.CAN-13-2470

Published OnlineFirst March 27, 2014; DOI: 10.1158/0008-5472.CAN-13-2470

germline control, DNA was obtained from bone marrow blood, peripheral blood, or bone marrow smears in which absence of tumor cells was pathologically confirmed. Bone marrow smears were used as normal samples for cases 05, 07, 08, and 12. This study was approved by The University of Tokyo Ethics Committee (Tokyo, Japan; approval number 1598), and informed consent was obtained from the parents of all participants.

Whole-exome sequencing

Whole-exome sequencing of primary tumor and matched normal specimens of cases 01, 02, 04, 07, 09, 10, and 12 was performed as previously described (7, 8). Relapsed tumor specimens of cases 01 and 02 were also analyzed. Whole-exome capture was accomplished using liquid-phase hybridization of sonicated genomic DNA having a 150 to 200-bp mean length to a bait cRNA library synthesized on magnetic beads (SureSelect Human All Exon Kit V3 or V5, Agilent Technology) according to the manufacturer's protocol. The captured targets were subjected to sequencing using HiSeq 2000 (Illumina) according to the manufacturer's instructions. Raw sequence data were processed using Genomon-exome (http://genomon.hgc.jp/exome/en/index.html) for detection of cancer exome sequencing data through the in-house pipeline constructed at the Human Genome Center, the Institute of Medical Science, The University of Tokyo. Analyses using Genomon are summarized in Supplementary Fig. S1. Sequence data have been deposited at the European Genome-phenome Archive (EGA, http://www.ebi.ac.uk/ega/), which is hosted by the European Bioinformatics Institute, under accession number EGAS00001000662.

Deep sequencing for validation of variants detected by whole-exome sequencing

To validate the mutations detected by whole-exome sequencing, deep sequencing was performed using pair or trio DNA specimens (primary/relapse tumor and normal) using HiSeq 2000 or MiSeq (Illumina). Primers used for this validation are listed in Supplementary Table S1. Mutations were amplified using PCR with a *NotI* linker individually attached to each primer and pooled together on a per-sample basis after successful amplification was confirmed by gel electrophoresis. Pooling was followed by purification of DNA using the FastGene Gel/PCR Extraction Kit (Nippon Genetics) and digestion with *NotI*. The digested DNA was purified again, and an aliquot of purified DNA was ligated with T4 DNA ligase for 5 hours, sonicated into approximately 200 bp fragments on an average using Covaris (Covaris), and used for generation of sequencing libraries with the NEBNext Ultra DNA Library Prep Kit for Illumina (New England Biolabs) according to the manufacturer's protocol. Data processing was performed according to previously described methods (7, 8). Each single-nucleotide variant and each insertion/deletion (indel) whose variant allele frequency (VAF) in the tumor sample was equal to or more than 2.0% and in the germline sample less than 2.0% were assigned as a somatic mutation. If the mutant allele frequency in the matched nontumor sample was more than 2.0%, the mutation was discarded (8). The mutation was evaluated for pathogenicity using the online mutation predicting tool, Mutation Taster (http://www.mutationtaster.org).

Small RNA sequencing

RNA was extracted using the miRNeasy Kit (Qiagen). Total RNA was quantified and evaluated for quality using a bioanalyzer (Agilent Technology). Libraries for small RNA sequencing were generated using the TruSeq small RNA Sample Preparation Kit (Illumina) and analyzed using the Illumina MiSeq according to the manufacturer's protocol. Small RNA sequencing was performed for four cases (cases 01, 07, 08, and 09). Read sequences were aligned against miRBase (release 16) using MiSeq Reporter v2.3 (Illumina). After alignment, the number of read sequences aligned to each miRNA or pre-miRNA was calculated. Gurtan and colleagues demonstrated that the RNase IIIA and IIIB domains of DICER1 process the 3′ (3p) and 5′ (5p) arms of miRNAs, respectively, *in vivo* (9). We defined the pre-miRNA cleavage ratio as the read counts of miRNA/(read counts of pre-miRNA + miRNA). This ratio was calculated for 5p or 3p miRNA, and then compared tumor specimens with fetal lung as normal control. Statistical differences were calculated by Wilcoxon rank-sum test.

Single-nucleotide polymorphism genotyping microarray

DNA of 11 cases (excluding case 11) as well as that of three relapse cases was hybridized to Affymetrix GeneChip 250K Nsp arrays (Affymetrix). DNA of cases 10 (at relapse) and 11 was not hybridized because of the poor quality of DNA from the paraffin-embedded samples. After appropriate normalization of mean array intensities, signal ratios between tumors and anonymous normal references were calculated in an allele-specific manner, and allele-specific copy numbers were inferred from the observed signal ratios based on a hidden Markov model using CNAG software (http://www.genome.umin.jp).

Sanger sequencing and targeted deep amplicon sequencing

Sanger sequencing of *DICER1* and *TP53* was performed for samples from all cases and relapsed tumor samples from four cases. Germline DNA was sequenced for nine cases (including case 02 without *DICER1* mutation). Sanger sequencing of *PDCD2L* and *UBA2* was performed for 11 cases. Deep amplicon sequencing of target exons of *TP53*, *GPR182*, and *CTNNB1* was performed for 14 samples from 11 cases. Exons harboring mutations in *DICER1* were sequenced for 11 cases, and all coding exons of *DICER1* were sequenced for case 02. Details of deep sequencing have been provided above. All primer sequences for these genes are listed in Supplementary Table S2–S4.

Results

The mean coverage in the whole-exome sequencing of tumor and germline samples was 126× and 128× for the 50 Mb target regions, respectively. More than 93% of the coding sequences were represented by more than 20 independent reads on an average (Supplementary Fig. S2). GC content and mean coverage are shown in Supplementary Fig. S3. Mean coverage of high-GC (≥60%) exons was lower than that of low GC (<60%). In total, 217 nonsilent substitutions and 12 indels

Published OnlineFirst March 27, 2014; DOI: 10.1158/0008-5472.CAN-13-2470

were detected across nine tumor specimens, of which 191 (88%) and 12 (100%), respectively, were successfully confirmed by deep sequencing (Supplementary Table S5). The number of nonsilent mutations per sample at presentation (13–35 mutations) was lower than that reported in most solid tumors in adults (10–12), but comparable with the number reported for other pediatric tumors such as neuroblastoma and medulloblastoma (18 and 16, respectively; Fig. 1A; refs. 13, 14). In two cases for which serial samples could be analyzed, relapsed samples had higher mutation number than corresponding samples at initial presentation (Fig. 1A and B). In both cases, intratumoral subpopulations were evident at the time of initial presentation (Fig. 1C). As previously reported for other cancers (15, 16), the clonal architecture of tumor subpopulations underwent dynamic evolutionary alterations during tumor progression. Serial samples in each case had several clonal mutations in common as well as harbored private subclonal mutations of their own (Fig. 1B and C). In case 01, some of the subclonal mutations (purple) found in the initial sample disappeared at relapse and were replaced by new mutations carried by new subpopulations (red), whereas most of the mutations found in the subclones (green) were retained at similar relative allele frequencies in the relapse sample in case 02. In both cases, relapsed tumors were accompanied by newly acquired gene mutations in each subpopulation and/or by appearance of new subclones that were totally absent from the original initial samples (Fig. 1C).

DICER1 mutations were detected for six cases (cases 01, 04, 07, 09, 10, and 12) but not for case 02; targeted deep sequencing was unable to detect any *DICER1* mutations. *DICER1* mutations were found in the major tumor populations in these six cases (Fig. 1C and D). In contrast with previous reports where all *DICER1* mutations were heterozygous and had germline origin, we identified two homozygous somatic *DICER1* mutations in cases 09 and 10, prompting us to investigate the status of *DICER1* mutations in five additional cases. *DICER1* mutations were found in 11 of 12 (92%) cases (Table 1; Fig. 2A and Supplementary Fig. S4), in which six of the 11 cases with *DICER1* mutations carried compound heterozygous mutations. Two cases carried homozygous *DICER1* mutations (Fig. 2B), presumably caused by copy number-neutral LOH (or uniparental disomy; UPD) involving the 14q arm harboring the *DICER1* locus. In total, biallelic *DICER1* mutations were found in eight of the 11 (73%) cases with *DICER1* mutations. We failed to demonstrate biallelic alterations in three cases (case 01, 05, and 11; Table 1 and Supplementary Fig. S4). We confirmed the same *DICER1* mutation status in initial and relapse samples in all four cases, for which both serial samples were available, indicating that *DICER1* mutations are involved in tumor development rather than progression.

Germline DNA was available in eight cases to confirm germline/somatic origins of *DICER1* mutations, of which four (cases 04, 07, 08, and 12) were compound heterozygous for a germline nonsense/frameshift and a somatic missense mutation, two (cases 09 and 10) were homozygous for somatic, missense mutations caused by an acquired UPD, and the remaining cases were heterozygous for a somatic missense mutation (case 01) or a germline frameshift mutation (case 05;

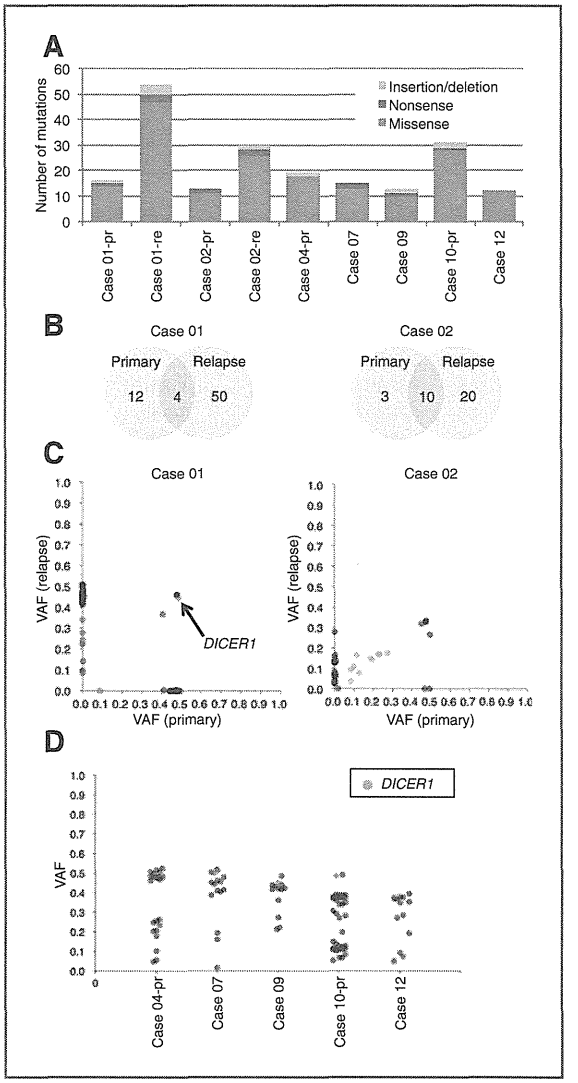

Figure 1. Mutations and mutant allele frequencies detected by whole-exome sequencing in 7 PPB cases. A, type and number of somatic mutations in each tumor. Each mutation type is distinguished using the indicated color. Primary (pr) and relapsed (re) tumors of cases 01 and 02 were examined independently by whole-exome sequencing. B, Venn diagram of somatic mutations found in cases 01 and 02. Both relapsed (re) tumors had increased number of somatic mutations compared with primary (pr) tumors. C, VAF distribution of validated mutations in relapsed cases. VAF was obtained from deep sequencing. Allele frequencies were corrected for copy numbers determined by SNP array analysis. *DICER1* mutation is discriminated by the indicated color in case 01. Case 02 harbored no *DICER1* mutation. Subclonal mutations in case 01 at primary (pr) and relapse (re) are distinguished by purple and red, respectively. Subclonal mutations in case 02 are distinguished by green. D, VAF distribution of validated mutations in nonrelapsed cases. *DICER1* mutations were included in the major tumor population.

Table 1). Among the three cases without normal samples, the combination of a nonsense and missense mutation was also found in the two cases with compound heterozygous mutations. In these cases, a somatic origin was suspected for a

Published OnlineFirst March 27, 2014; DOI: 10.1158/0008-5472.CAN-13-2470

Table 1. Mutations in *DICER1* and *TP53* in sporadic PPB cases

	DICER1				*TP53*				
Case	Exon	Mutation	AA change	Origin	Exon	Mutation	AA change	17p	Sample
01	25	5428G>T	D1810Y	Somatic		Native		Loss	Pr/Re
02		Native				Native			Pr/Re
03	23	4910C>A	S1637X	ND	4	c.332_333delTG	p.L111fs	Loss	Pr
	24	5114A>T	E1705V	ND					
04	21	3482delC	P1161fs	Germline	5	c.527G>T[a]	p.C176F	Loss	Pr/Re
	24	5125G>A	D1709N	Somatic	4	c.313G>A[b]	p.G105S		
05	9	1383delAAAG	I461fs	Germline		Native			Pr
06	19	3007C>T	R1003X	ND		Native			Pr
	25	5428G>T	D1810Y	Probably somatic					
07	18	2863insA	T955fs	Germline	8	c.891_903	p.H297fs	Loss	Pr
	25	5425G>A	G1809R	Somatic		delCGAGCTGCCCCCA			
08	21	3748delC	S1250fs	Germline	7	c.762_764delACAT	p.I254fs	Loss	Pr
	25	5425G>A	G1809R	Somatic					
09	25	5425G>A (Homozygous)	G1809R	Somatic		Native		Loss	Pr
10	25	5425G>A (Homozygous)	G1809R	Somatic	8	c.817C>T	p.R273C	Loss	Pr/Re
11	8	1148dupAGGGT	I383fs	ND		Native		ND	Pr
12	25	5460C>G	Y1820X	Germline		Native		Loss	Pr
	25	5438A>G	E1813G	Somatic					

Abbreviations: ND, not determined; AA, amino acid; Pr, primary; Re, relapse.

[a]Primary tumor.

[b]Relapse tumor.

missense mutation (D1810Y) in case 06, in that the VAF of that mutant deviated significantly from the expected value (0.5) for germline variants (Supplementary Table S6). Conspicuously, all the nine missense *DICER1* mutations found in our cohort were located within the RNase IIIb domain with a mutational hotspot at G1809 (Fig. 2C), for which a somatic origin was confirmed or highly suspected in eight mutations. Combined with previous reports for PPB (2, 3), this high frequency of germline mutations supported the incomplete penetrance of *DICER1* mutations in both familial and sporadic PPB. To assess the effect of *DICER1* mutation in RNase IIIb domain on RNA cleavage, we performed small RNA sequencing in tumors with mutational hotspots at G1809R and D1810Y. Total RNA including miRNA extracted from fetal lung was used as a normal control. Given that the RNase IIIA and IIIB domains of DICER1 process the 3p and 5p arms of miRNAs, respectively (9), *DICER1* mutations in RNase IIIb domain are expected to affect 5p rather than 3p miRNA expression. Comparing the pre-miRNA cleavage ratio of tumor samples to that of the fetal lung control, we confirmed dramatically reduced 5p miRNA expression in the tumors with G1809R and D1810Y mutations ($P < 7.1 \times 10^{-7}$; Fig. 3A and B). In contrast, 3p miRNA expression was significantly higher in the tumor samples than in fetal lung control ($P < 1.4 \times 10^{-3}$), suggesting that G1809R and D1810Y mutants have opposite effects on 3p miRNA cleavage. Taken together, our results suggest that a mutational hotspot at G1809R has a pathogenic effect.

Except for *DICER1*, several genes were found to be recurrently mutated in whole-exome sequencing, including *TP53*, *CTNNB1*, *GPR182*, *MYH8*, *PDE2A*, and *TMX3* (Supplementary Table S7). *TP53*, *CTNNB1*, and *GPR182* were investigated by targeted deep sequencing in an additional five cases, although these genes were not mutated in *CTNNB1* and *GPR182*. The result of targeted deep sequencing in *TP53* is described below. To identify additional genetic alterations, we next performed single-nucleotide polymorphism (SNP) array-based genome-wide copy number analysis in 14 samples of 11 cases for which high-quality genomic DNA was available (including three cases with both primary and relapsed tumors). Chromosome 8q gain was the most common copy number change and was found in 10 of the 11 cases in varying combinations with other genetic changes, including loss of chromosomes 10 and 17p and high-grade amplification of 19q (Fig. 4A and Supplementary Figs. S4 and S5). Chromosome 17p LOH was found in 10 samples and was caused by UPD ($N = 1$) or deletions ($N = 9$), and commonly involved an 8.5-Mb region that contained *TP53*. To investigate a possible role of *TP53* mutations in PPB, we analyzed the *TP53* mutation status in 14 tumor samples from all 12 cases by Sanger and deep sequencing. We detected recurrent missense or frame shift mutations in five of the 12 cases (42%; Fig. 4B; Table 1), in which all five cases were accompanied by 17p LOH and led to biallelic *TP53* inactivation. Intriguingly, in case 04, the relapsed tumor had a different *TP53* mutation (G105S) from that found at the time of initial presentation (C176F), suggesting that the relapse originated from a different subclone in which the two *DICER1* mutations predated *TP53* mutations. We also found several focal amplifications involving 5q23, 6q16-21, 15q23-24, and 19q13.11. However, none of

Published OnlineFirst March 27, 2014; DOI: 10.1158/0008-5472.CAN-13-2470

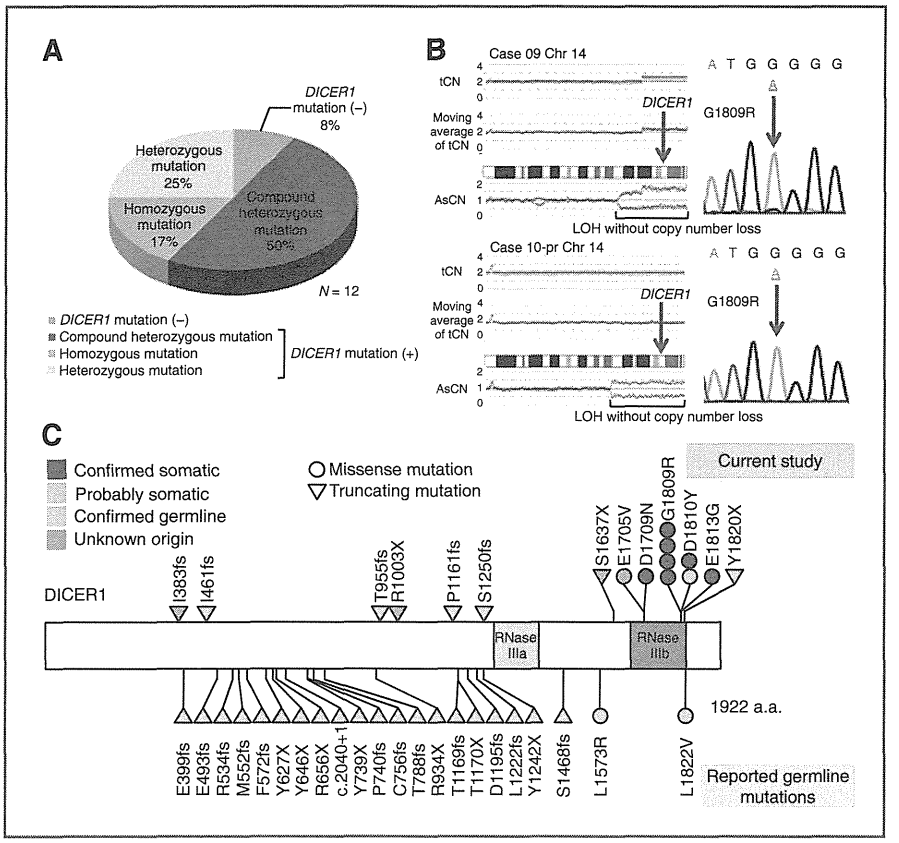

Figure 2. DICER1 abnormalities detected in 12 PPB cases. A, frequency of identified *DICER1* mutations in 12 cases. B, homozygous *DICER1* mutation with 14q LOH without copy number loss. Right panels show a sequence chromatogram of a G1809R homozygous mutation. Left panels show 14q LOH obtained from SNP array analysis. tCN, total copy number; AsCN, allele-specific copy number. C, a schematic of DICER1 protein structure with the positions of alterations. Top and bottom portions indicate mutations detected in our study and previously reported mutations in references 2 and 3, respectively. All the nine missense *DICER1* mutations found in our cohort were located within the RNase IIIb domain with a mutational hotspot at G1809. fs, frameshift.

these amplifications were recurrent, except for those involving 19q13.11, which were found in three (25%) of the 12 cases (Supplementary Fig. S5). The amplified region contains five genes, including *LSM14A*, *KIAA0355*, *GPI*, *UBA2*, and *PDCD2L*, but mutations were detected in none of these genes.

Discussion

The most striking discovery in the present study is the frequent biallelic involvement of *DICER1* mutations in majority of PPB cases with an obligatory missense mutation involving the RNase IIIb domain. In our cohort, biallelic *DICER1* mutations were documented in eight of the 11 *DICER1*-mutated cases with sporadic PBB, with RNase IIIb domain-involving mutations found in all cases and somatic origins demonstrated in all evaluable cases. This result was in stark contrast with previous reports, where all *DICER1* mutations in PPB or *DICER1* syndrome cases were heterozygous and inherited from parents; all mutations were either nonsense or frameshift changes except for two cases, of which one had a missense mutation in the RNase III domain (2, 3). Interestingly, a recent study reported frequent recurrent *DICER1* mutations affecting the RNase IIIb domain in nonepithelial ovarian cancers, especially Sertoli–Leydig cell tumor, in which 26 of 43 tumors carried exclusively RNase IIIb domain mutations with only four tumors being compound heterozygotes of a germline nonsense/frameshift mutation and an RNase IIIb domain mutation (5). Conspicuously, no germline mutations involving the RNase IIIb domain and no biallelic nonsense or frameshift mutations have been reported in any human cancers, possibly accounting for the different spectrum of *DICER1* mutations between PPB and ovarian cancers. These unique features of *DICER1* mutations suggest distinct oncogenic roles of both nonsense/frameshift and RNase IIIb domain mutations. It could be hypothesized that complete loss of DICER1 functions caused by biallelic nonsense/frameshift mutations is not compatible with cell viability, whereas further loss of particular DICER function, beyond haploinsufficiency through targeted mutations within the RNase IIIb domain, could be required or effective for the tumor cells to be clonally selected.

The RNase IIIb domain in DICER1 and other RNase III protein family members is involved in excision of double-stranded miRNA stems, which are then cleaved to single-stranded miRNA through the activity of the RNase IIIa domain (5). A mutation of the conserved amino acids in the RNase IIIb domain could thus lead to compromised miRNA processing, especially in excision of miRNAs. In fact, four mutational hotspots at metal-binding sites (E1705, D1709, D1810, and E1813) found in nonepithelial ovarian cancer were shown to have decreased RNase IIIb activity (5). In the current study, we found an additional mutational hotspot within the RNase IIIb domain affecting a highly conserved amino acid position

Published OnlineFirst March 27, 2014; DOI: 10.1158/0008-5472.CAN-13-2470

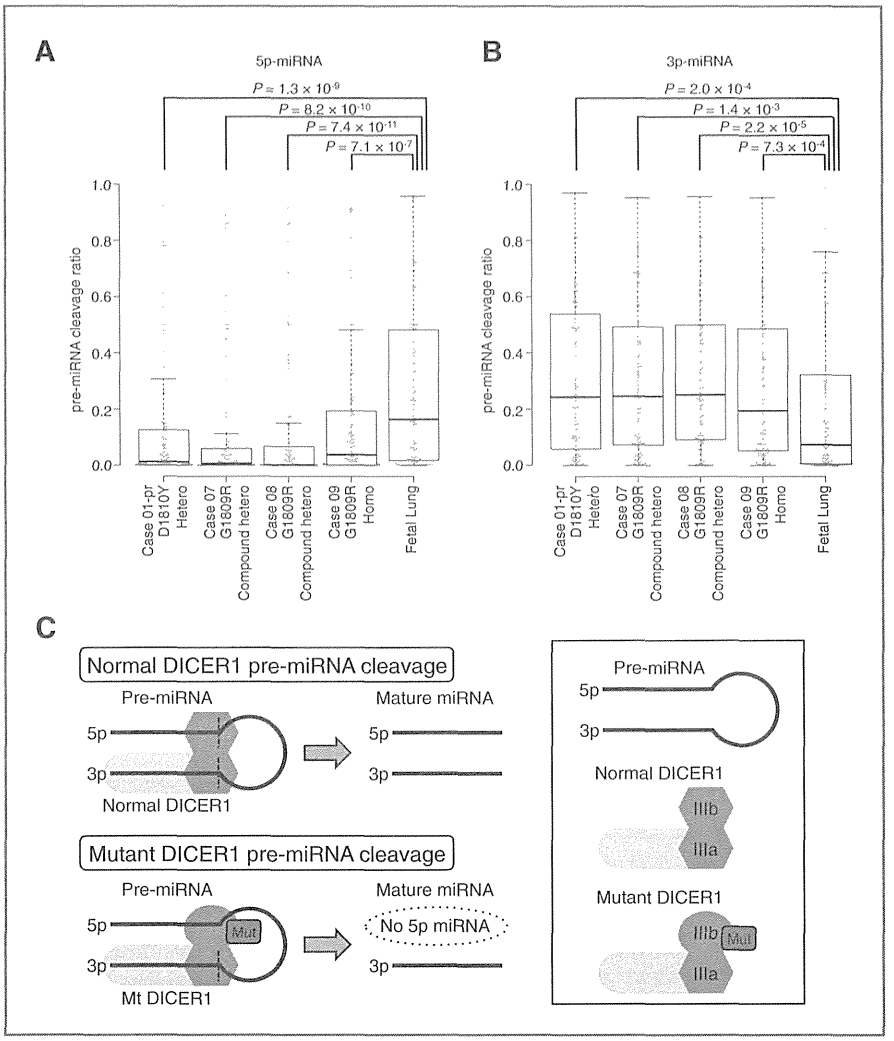

Figure 3. Significant reduction of pre-miRNA cleavage of 5p strand in four tumor specimens by small RNA sequencing. A, 5p miRNA biogenesis was significantly reduced in tumor samples. *P* values were calculated by Wilcoxon rank-sum test. B, 3p miRNA biogenesis was retained in tumor samples. In contrast with 5p miRNA expression, 3p miRNA expression in tumor samples exceeds normal control. C, schematic model of aberrant pre-miRNA cleavage by hotspot mutant DICER1. The miRNA biogenesis pathway by normal DICER1 is indicated in the top panel. A proposed model of hotspot DICER1 mutant is presented in the lower panel. Hotspot DICER1 mutant could not cleave the 5p strand of pre-miRNA. Loss of 5p miRNA may prompt DICER1 to cleave pre-miRNA so that 3p miRNA may be overprocessed.

(G1809) in the vicinity of the two known hotspot codons (D1810 and E1813). Our small RNA sequencing revealed that mutational hotspots at G1809 and a D1810 mutation showed a dramatically reduced cleavage ratio of 5p miRNA, and D1810 mutation also showed the same results in PPB. D1810 mutation is one of the hotspot mutations in nonepithelial ovarian cancer (5), of which reduced 5p miRNA expression has been already confirmed (17). This finding suggests that a specific mutational hotspot of PPB, G1809, is functionally equivalent to hotspot mutations in nonepithelial ovarian cancer. Anglesio and colleagues showed no significant change in 3p miRNA expression (17); however, its cleavage ratio was increased in our analysis. This result may be due to the existence of some mechanism that activates DICER1 to compensate the loss of 5p miRNA production (Fig. 3C). Gurtan and colleagues also mentioned an increased ratio of miRNA star to mature strands relative to cells expressing native hsDicer (9). MiRNA star means less abundant mature miRNA, which usually consists of 3p miRNA, so that this result is compatible with our observation. Thus, it seems that mutations at G1809 could lead to a biologic consequence similar to that of known hotspot mutations (5), although the oncogenic mechanism of the defective cleavage but not excision of miRNAs in the pathogenesis of PPB and other cancers awaits elucidation.

Besides *DICER1* mutations, *TP53* mutations with or without 17p loss as well as trisomy 8 and other chromosomal abnormalities were among the common genetic lesions in PPB. With respect to *DICER1* mutations, it is of note that TP53 also plays a critical role in the regulation of miRNA processing (18). Indeed, tumor-derived transcriptionally inactive TP53 mutants suppress precursor and mature miRNA levels, whereas native TP53 increases them (18), indicating that *TP53* plays an important role in cancer biology via regulation of miRNA processing. A recent study showed that TP53 regulates DICER1 expression via transcriptional miRNAs such as let-7 (19). In contrast, Wang and colleagues showed that knockdown of *DICER1*

Published OnlineFirst March 27, 2014; DOI: 10.1158/0008-5472.CAN-13-2470

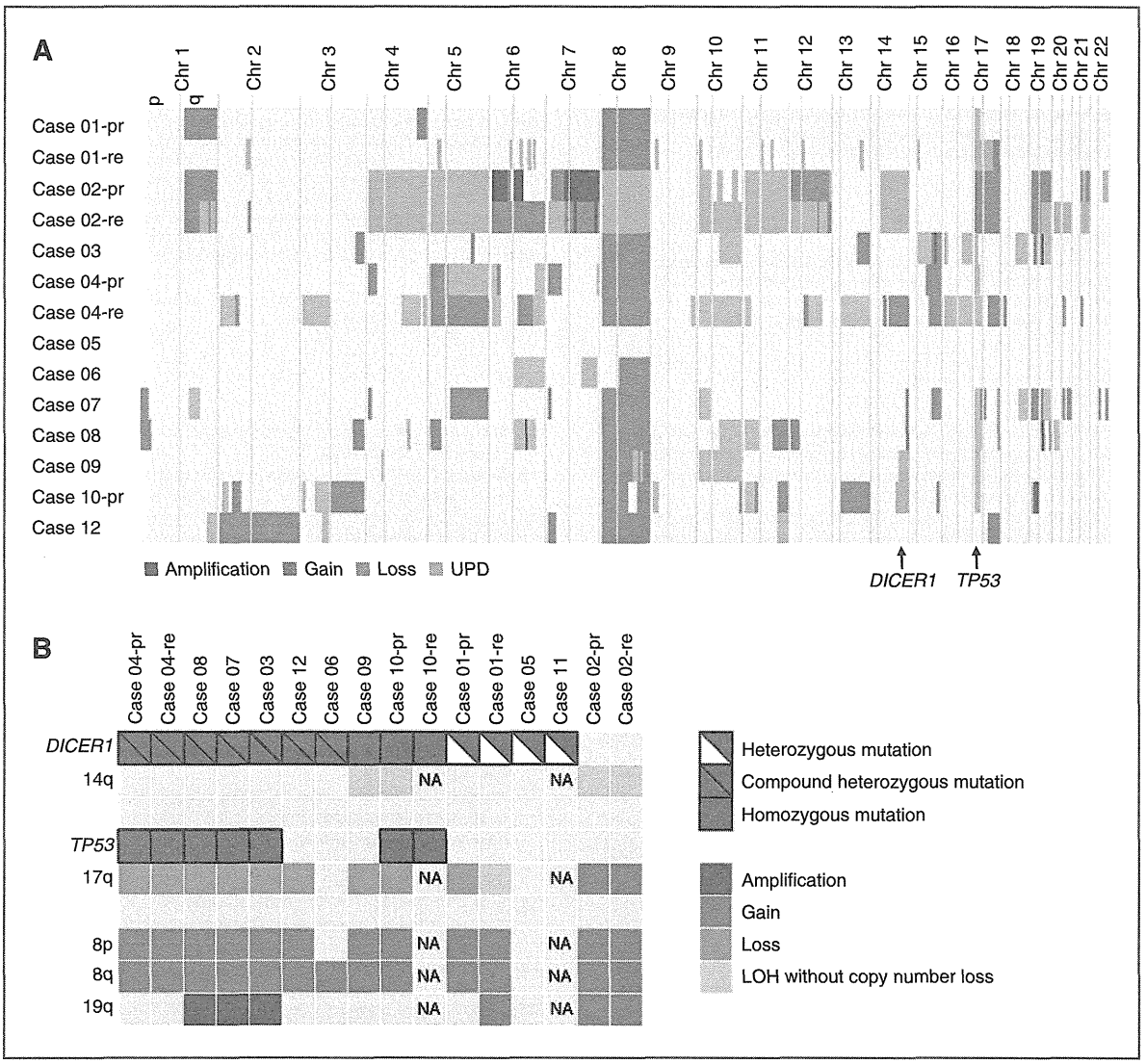

Figure 4. Overview of *DICER1* and *TP53* mutations with copy number alterations. A, copy number alterations by SNP array analysis in 14 PPB samples from 11 cases. The regions of *DICER1* and *TP53* are indicated by arrows. Amplification, gain, loss, and UPD are distinguished by the indicated colors. Copy number (CN) gain was defined as copy number between 3 and 5. Amplification was defined as an inferred copy number of more than 5. Copy number loss was defined as copy number less than one copy and LOH was assigned when one allele was retained. B, distribution of *DICER1* and *TP53* mutations with frequently detected copy number alterations. pr, primary; re, relapse; NA, not available.

expression in BxPC-3 and Panc-1 pancreatic cancer cells resulted in significant increases in TP53 protein levels (20), suggesting the existence of a regulatory loop between TP53, DICER1, and let-7, deregulation of which may play a role in PPB development.

In conclusion, biallelic *DICER1* mutations were common in PPB, invariably accompanied by a somatic RNase IIIb domain mutation. Majority of cases had mutated *DICER1* alleles in germline with or without an additional RNase IIIb domain mutation in the remaining allele. Recurrent mutations were rare in PPB, except for frequent *TP53* deletions/mutations. Our results provide novel insight into the critical role of *DICER1* mutations and importance of *TP53* inactivation in the pathogenesis of PPB.

Disclosure of Potential Conflicts of Interest

No potential conflicts of interest were disclosed.

Authors' Contributions

Conception and design: M. Seki, S. Ogawa, J. Takita
Development of methodology: Y. Shiraishi, Y. Okuno
Acquisition of data (provided animals, acquired and managed patients, provided facilities, etc.): M. Seki, K. Yoshida, Y. Sato, R. Nishimura, Y. Okuno, K. Kato, R. Hanada, Y. Nomura, M.-J. Park, T. Ishida

Published OnlineFirst March 27, 2014; DOI: 10.1158/0008-5472.CAN-13-2470

Analysis and interpretation of data (e.g., statistical analysis, biostatistics, computational analysis): M. Seki, Y. Shiraishi, T. Shimamura, Y. Sato, Y. Okuno, K. Chiba, H. Tanaka, S. Miyano
Writing, review, and/or revision of the manuscript: M. Seki, A. Oka, S. Ogawa, J. Takita
Administrative, technical, or material support (i.e., reporting or organizing data, constructing databases): T. Ishida, Y. Hayashi
Study supervision: T. Igarashi, Y. Hayashi, S. Ogawa, J. Takita

Acknowledgments

The authors thank Matsumura, Hoshino, Yin, Saito, Mori, Nakamura, Mizota, and Drs. K. Ohki and J. Okubo for excellent technical assistance and Drs. Y. Tanaka, K. Ida, A. Motomura, R. Shiozawa, K. Watanabe, and A. Kozaki for assisting with clinical care for patients and collecting samples.

Grant Support

This work was supported by Research on Measures for Intractable Diseases, Health, and Labor Sciences Research Grants, the Ministry of Health, Labour and Welfare; Research on Health Sciences focusing on Drug Innovation; the Japan Health Sciences Foundation, grant from the Ministry of Education, Culture, Sports, Science and Technology of Japan, KAKENHI (22134006), the Project for the Development of Innovative Research on Cancer Therapeutics (P-DIRECT), and also by the Japan Society for the Promotion of Science through the "Funding Program for World-Leading Innovative R&D on Science and Technology (FIRST Program)," initiated by the Council for Science and Technology Policy.

The costs of publication of this article were defrayed in part by the payment of page charges. This article must therefore be hereby marked *advertisement* in accordance with 18 U.S.C. Section 1734 solely to indicate this fact.

Received August 27, 2013; revised February 17, 2014; accepted March 9, 2014; published OnlineFirst March 27, 2014.

References

1. Hill DA, Jarzembowski JA, Priest JR, Williams G, Schoettler P, Dehner LP. Type I pleuropulmonary blastoma: pathology and biology study of 51 cases from the international pleuropulmonary blastoma registry. Am J Surg Pathol 2008;32:282–95.
2. Hill DA, Ivanovich J, Priest JR, Gurnett Ca, Dehner LP, Desruisseau D, et al. DICER1 mutations in familial pleuropulmonary blastoma. Science 2009;325:965.
3. Slade I, Bacchelli C, Davies H, Murray a, Abbaszadeh F, Hanks S, et al. DICER1 syndrome: clarifying the diagnosis, clinical features and management implications of a pleiotropic tumour predisposition syndrome. Am J Med Genet 2011;48:273–8.
4. Carthew RW. Gene regulation by microRNAs. Curr Opin Genet Dev 2006;16:203–8.
5. Heravi-Moussavi A, Anglesio MS, Cheng SW, Senz J, Yang W, Prentice L, et al. Recurrent somatic DICER1 mutations in nonepithelial ovarian cancers. N Engl J Med 2012;366:234–42.
6. Kumar MS, Pester RE, Chen CY, Lane K, Chin C, Lu J, et al. Dicer1 functions as a haploinsufficient tumor suppressor. Genes Dev 2009;23:2700–4.
7. Yoshida K, Sanada M, Shiraishi Y, Nowak D, Nagata Y, Yamamoto R, et al. Frequent pathway mutations of splicing machinery in myelodysplasia. Nature 2011;478:64–9.
8. Yoshida K, Toki T, Okuno Y, Kanezaki R, Shiraishi Y, Sato-Otsubo A, et al. The landscape of somatic mutations in Down syndrome-related myeloid disorders. Nat Genet 2013;45:1293–9.
9. Gurtan AM, Lu V, Bhutkar A, Sharp PA. *In vivo* structure-function analysis of human Dicer reveals directional processing of precursor miRNAs. RNA 2012;18:1116–22.
10. Banerji S, Cibulskis K, Rangel-Escareno C, Brown KK, Carter SL, Frederick AM, et al. Sequence analysis of mutations and translocations across breast cancer subtypes. Nature 2012;486:405–9.
11. Network CGAR. Integrated genomic analyses of ovarian carcinoma. Nature 2011;474:609–15.
12. Network CGAR. Comprehensive genomic characterization of squamous cell lung cancers. Nature 2012;489:519–25.
13. Pugh TJ, Weeraratne SD, Archer TC, Pomeranz Krummel DA, Auclair D, Bochicchio J, et al. Medulloblastoma exome sequencing uncovers subtype-specific somatic mutations. Nature 2012;488:106–10.
14. Pugh TJ, Morozova O, Attiyeh EF, Asgharzadeh S, Wei JS, Auclair D, et al. The genetic landscape of high-risk neuroblastoma. Nat Genet 2013;45:279–84.
15. Ding L, Ley TJ, Larson DE, Miller CA, Koboldt DC, Welch JS, et al. Clonal evolution in relapsed acute myeloid leukaemia revealed by whole-genome sequencing. Nature 2012;481:506–10.
16. Nik-Zainal S, Van Loo P, Wedge DC, Alexandrov LB, Greenman CD, Lau KW, et al. The life history of 21 breast cancers. Cell 2012;149:994–1007.
17. Anglesio MS, Wang Y, Yang W, Senz J, Wan A, Heravi-Moussavi A, et al. Cancer-associated somatic DICER1 hotspot mutations cause defective miRNA processing and reverse-strand expression bias to predominantly mature 3p strands through loss of 5p strand cleavage. J Pathol 2013;229:400–9.
18. Suzuki HI, Yamagata K, Sugimoto K, Iwamoto T, Kato S, Miyazono K. Modulation of microRNA processing by p53. Nature 2009;460:529–33.
19. Lujambio A, Lowe SW. The microcosmos of cancer. Nature 2012;482:347–55.
20. Wang X, Zhao J, Huang J, Tang H, Yu S, Chen Y. The regulatory roles of miRNA and methylation on oncogene and tumor suppressor gene expression in pancreatic cancer cells. Biochem Biophys Res Commun 2012;425:51–7.

Published OnlineFirst March 27, 2014; DOI: 10.1158/0008-5472.CAN-13-2470

AACR American Association for Cancer Research

Cancer Research

The Journal of Cancer Research (1916–1930) | The American Journal of Cancer (1931–1940)

Biallelic *DICER1* Mutations in Sporadic Pleuropulmonary Blastoma

Masafumi Seki, Kenichi Yoshida, Yuichi Shiraishi, et al.

Cancer Res 2014;74:2742-2749. Published OnlineFirst March 27, 2014.

Leukemia (2014) **28**, 1844–1850

www.nature.com/leu

ORIGINAL ARTICLE

Haploinsufficiency of *Sf3b1* leads to compromised stem cell function but not to myelodysplasia

M Matsunawa[1,6], R Yamamoto[2,6], M Sanada[1,6], A Sato-Otsubo[1], Y Shiozawa[1], K Yoshida[1], M Otsu[2], Y Shiraishi[3], S Miyano[3,4], K Isono[5], H Koseki[5], H Nakauchi[2,7] and S Ogawa[1,7]

SF3B1 is a core component of the mRNA splicing machinery and frequently mutated in myeloid neoplasms with myelodysplasia, particularly in those characterized by the presence of increased ring sideroblasts. Deregulated RNA splicing is implicated in the pathogenesis of *SF3B1*-mutated neoplasms, but the exact mechanism by which the *SF3B1* mutation is associated with myelodysplasia and the increased ring sideroblasts formation is still unknown. We investigated the functional role of SF3B1 in normal hematopoiesis utilizing *Sf3b1* heterozygous-deficient mice. *Sf3b1*$^{+/-}$ mice had a significantly reduced number of hematopoietic stem cells ($CD34^-cKit^+Scal^+Lin^-$ cells or $CD34^-$KSL cells) compared with *Sf3b1*$^{+/+}$ mice, but hematopoiesis was grossly normal in *Sf3b1*$^{+/-}$ mice. When transplanted competitively with *Sf3b1*$^{+/+}$ bone marrow cells, *Sf3b1*$^{+/-}$ stem cells showed compromised reconstitution capacity in lethally irradiated mice. There was no increase in the number of ring sideroblasts or evidence of myeloid dysplasia in *Sf3b1*$^{+/-}$ mice. These data suggest that *SF3B1* plays an important role in the regulation of hematopoietic stem cells, whereas *SF3B1* haploinsufficiency itself is not associated with the myelodysplastic syndrome phenotype with ring sideroblasts.

Leukemia (2014) **28,** 1844–1850; doi:10.1038/leu.2014.73

INTRODUCTION

Frequent pathway mutations involving multiple components of the RNA splicing machinery are a cardinal feature of myeloid neoplasms, particularly those showing myeloid dysplasia in which the major mutational targets include *SF3B1*, *U2AF1*, *SRSF2* and *ZRSR2*.[1–4] *SF3B1* mutations are one of the most common genetic alterations in myelodysplastic syndromes (MDS) and have also been reported in 5 – 15% of chronic lymphocytic leukemia cases,[5] and at lower frequencies in a variety of solid cancers such as endometrial cancers,[2] pancreatic carcinoma,[6] breast cancers[7] and uveal melanoma.[8] *SF3B1* mutations are considered to be one of the founding genetic events in MDS and define a benign clinical phenotype.[2,9] The frequency of *SF3B1* mutations is particularly high among the unique subtypes of MDS that are characterized by increased ring sideroblasts, such as refractory anemia with ring sideroblasts (RARS) or refractory cytopenia with multiple lineage dysplasia with ring sideroblasts as well as RARS associated with thrombocytosis[9,10] in which mutation frequencies of 66.7 – 79% have been reported. These genetic findings strongly suggest a close relationship between *SF3B1* mutation and the presence of ring sideroblasts. However, the molecular mechanism by which *SF3B1* mutation leads to myelodysplasia and promotes the formation of ring sideroblasts is unknown.

SF3B1 encodes subunit 1 of the splicing factor 3b complex that is a core component of U2 small nuclear ribonucleoprotein. The U2 small nuclear ribonucleoprotein complex recognizes the 3′ splice site at intron–exon junctions in normal pre-mRNA splicing machinery,[11] in which SF3B1 is involved in recognition of the branchpoint sequence. It has been demonstrated that *Sf3b1* knockout mice are embryonic lethal at very early stages, whereas *Sf3b1* heterozygous knockout (*Sf3b1*$^{+/-}$) mice exhibit mild skeletal alterations.[12] However, a detailed analysis of the functional role of *Sf3b1* in hematopoiesis in these mice has not been reported.

In this study we investigated the hematological phenotype of *Sf3b1*$^{+/-}$ mice to clarify the role of *SF3B1* in hematopoiesis and to obtain insights into how deregulation of *SF3B1* leads to the development of MDS phenotypes.

MATERIALS AND METHODS

Ethical approval of the study protocol

Animal experiments were undertaken with the approval of the Animal Care and Use Committee of the Institute of Medical Science, University of Tokyo (Tokyo, Japan).

Mice

Generation of *Sf3b1*$^{+/-}$ mice was as previously described.[12] C57BL/6(CD45.1$^+$) mice and C57BL/6 F1-CD45.1$^+$CD45.2$^+$ mice were purchased from Japan SLC (Shizuoka, Japan) and Sankyo-Lab Service (Tsukuba, Japan), respectively.

Iron staining

Prussian blue stain (Muto Pure Chemicals, Tokyo, Japan) and nuclear red counterstain with nuclear fast red were performed by standard procedures. Light microscopic images were acquired on an OLYMPUS BX45 microscope

[1]Departments of Pathology and Tumor Biology, Graduate School of Medicine, Kyoto University, Kyoto, Japan; [2]Division of Stem Cell Therapy, Center for Stem Cell Biology and Medicine, Institute of Medical Science, University of Tokyo, Tokyo, Japan; [3]Laboratory of DNA Information Analysis, Human Genome Center, Institute of Medical Science, The University of Tokyo, Tokyo, Japan; [4]Laboratory of Sequence Analysis, Human Genome Center, Institute of Medical Science, The University of Tokyo, Tokyo, Japan and [5]Laboratory for Developmental Genetics, RIKEN Research Center for Integrative Medical Sciences, Yokohama, Japan. Correspondence: Dr S Ogawa, Departments of Pathology and Tumor Biology, Kyoto University, Yoshida Konoe-cho, Sakyo-ku, Kyoto 606-8501, Japan.
E-mail: sogawa-tky@umin.ac.jp
[6]These authors contributed equally to this work.
[7]These authors jointly directed this work.
Received 27 January 2014; accepted 10 February 2014; accepted article preview online 18 February 2014; advance online publication, 25 March 2014

and an OLYMPUS DP25 camera using DP2-BSW software (version 2.2; Olympus, Tokyo, Japan).

Colony-forming assays

Bone marrow (BM) cells (2.5×10^4 cells) from *Sf3b1*$^{+/-}$ or *Sf3b1*$^{+/+}$ mice at the age of 8 weeks were seeded into methylcellulose-containing medium (MethoCult M3234; Stem Cell Technologies, Vancouver, BC, Canada) supplemented with 10 ng/ml murine interleukin-3, 10 ng/ml murine interleukin-6, 20 ng/ml murine thrombopoietin, 50 ng/ml murine stem cell factor (Wako Pure Chemical, Osaka, Japan) and 3 U/ml human recombinant erythropoietin (R&D Systems, Minneapolis, MN, USA). The number of colonies was counted after 14 days of culture.

Flow cytometry

Measurement of hematopoietic stem cells (HSCs) and hematopoietic progenitor cells was conducted in 8-week-old male mice as previously described.[13] Stained cells were analyzed with FACSAria II or FACSCanto II flow cytometers (BD Bioscience, Franklin Lakes, NJ, USA). Cell sorting was performed on a MoFlo system (Beckman Coulter, Fullerton, CA, USA). Data were analyzed by FlowJo software (Tree Star, Ashland, CA, USA). The antibodies used in this study are listed in the Supplementary Table 1.

Competitive repopulation assay

Unfractionated pooled BM cells (1×10^6 cells) from 8-week-old *Sf3b1*$^{+/-}$ or *Sf3b1*$^{+/+}$ mice (CD45.2$^+$) were transplanted into 8–12-week-old female CD45.1$^+$ recipient mice lethally irradiated at 2 doses of 4.9 Gy together with the same number of BM cells from 8–12-week-old male CD45.1$^+$/CD45.2$^+$ mice as competitors. Sorted 120 CD34$^-$KSL cells as well as 80 CD150$^+$CD34$^-$KSL cells obtained from *Sf3b1*$^{+/-}$ or *Sf3b1*$^{+/+}$ mice were transplanted into lethally irradiated recipients together with competitor whole BM cells (5×10^5 cells). At 40 weeks after transplantation, BM cells (1×10^7) were harvested from the recipient mice and were serially transplanted into second recipients. The chimerism of donor-derived cells was evaluated by flow cytometry as previously described.[14] The antibodies used in this study are listed in the Supplementary Table 1.

Gene expression analyses

Total RNA was prepared from CD34$^-$KSL cells, pooled from 3 female mice at the age of 11–13 weeks, using NucleoSpin RNA XS (Macherey-Nagel, Düren, Germany). For RNA sequencing analyses, the synthesis and amplification of complementary DNA was done using a SMARTer Ultra Low RNA kit for Illumina sequencing (Clontech Laboratories, Mountain View, CA, USA) according to the manufacturer's protocol. Sequencing libraries were generated using the NEBNext DNA Library Prep Reagent Set for Illumina (New England BioLabs, Ipswich, MA, USA) and analyzed using Illumina HiSeq 2000 (Illumina, San Diego, CA, USA) according to the manufacturer's protocol. Data processing was performed as described previously.[1,15] All sequence reads were mapped to the mouse transcriptome based on the UCSC known gene (downloaded in June 2013) using bowtie ver. 0.12.7 (http://bowtie-bio.sourceforge.net/index.shtml),[16] and unmapped or poorly mapped reads were realigned to mouse reference genome (mm10) using BLAT (http://genome.ucsc.edu/).[17] The expression level of each transcript was quantified with normalized fragments per kilobase of transcript per million fragments sequenced[18] that were calculated using bedtools ver. 2.17.0 (https://code.google.com/p/bedtools/)[19] with a transcriptome reference (RefSeq Genes, downloaded in June 2013). Gene set enrichment analyses (GSEA) were performed with GSEA[20] ver. 2.0.13 software from the Broad Institute (http://www.broad.mit.edu/gsea). For quantitative reverse transcriptase-PCR, RNA was subjected to reverse transcription using the ReverTra Ace qPCR RT kit (Toyobo, Osaka, Japan) according to the manufacturer's protocol. Quantitative expression levels of mRNA were measured as described previously.[1,15] Primers used for quantitative reverse transcriptase-PCR are listed in the Supplementary Table 2.

Statistical analyses

Statistical significance was evaluated by Student's *t*-test, and $P<0.05$ was considered significant.

Table 1. Peripheral blood counts of *Sf3b1*$^{+/+}$ and *Sf3b1*$^{+/-}$ mice at 8 weeks

Parameter	*Sf3b1*$^{+/+}$	*Sf3b1*$^{+/-}$	N	P-*value*
WBC count ($\times 10^4/\mu l$)	1.32 ± 0.56	1.09 ± 0.28	6	0.39
Neutrophil (%)	13.67 ± 6.40	15.83 ± 6.28	6	0.57
Lymphocyte (%)	80.58 ± 7.14	79.08 ± 6.50	6	0.71
Monocyte (%)	5.75 ± 1.54	5.08 ± 2.84	6	0.62
Hb level (g/dl)	18.23 ± 1.37	17.61 ± 1.00	6	0.39
PLT ($\times 10^4/\mu l$)	110.63 ± 22.68	119.30 ± 18.44	6	0.48

Abbreviations: Hb, hemoglobin; PLT, platelets; WBC, white blood cells. Data are the mean ± s.d. ($n = 6$).

RESULTS

Hematologic findings are not disturbed in *Sf3b1*$^{+/-}$ mice

No *Sf3b1*-null mice were obtained, confirming the previous observation that *Sf3b1*$^{-/-}$ mice should be embryonic lethal. However, *Sf3b1*$^{+/-}$ mice were obtained at an expected frequency compared with *Sf3b1*$^{+/+}$ littermates and appeared grossly normal.[12] The complete peripheral blood counts in *Sf3b1*$^{+/-}$ mice at 8 weeks of age were comparable with those in *Sf3b1*$^{+/+}$ littermate mice with normal differential counts of white blood cells (Table 1). There was no significant change in the peripheral blood counts between *Sf3b1*$^{+/+}$ and *Sf3b1*$^{+/-}$ mice at any time points up to 54 weeks (Supplementary Figures 1a and b). *Sf3b1*$^{+/-}$ mice did not show any significant differences in total BM cellularity or the number of megakaryocytes, and their lineage composition was comparable with that of *Sf3b1*$^{+/+}$ mice (Table 2). No splenomegaly was observed in any mice tested in these experiments, and spleen weights were also similar to those of *Sf3b1*$^{+/+}$ mice (Table 2). No significant morphologic abnormalities were recognized in peripheral blood and BM cells in May–Grünwald–Giemsa staining. Taken together, these findings suggested that steady-state hematopoiesis was maintained almost normally in *Sf3b1*$^{+/-}$ mice.

The number of ring sideroblasts is not increased in *Sf3b1*$^{+/-}$ mice

To determine whether loss of *Sf3b1* alone can lead to increased production of ring sideroblasts, we examined cytospin BM specimens by Prussian blue staining for iron. In contrast to the previous report describing increased formation of ring sideroblasts in the same *Sf3b1*$^{+/-}$ strain of mouse,[21] we observed very few sideroblasts characterized by nuclei encircled by a small number of iron granules. Specifically, there was no significant difference in the number of sideroblasts between *Sf3b1*$^{+/-}$ and *Sf3b1*$^{+/+}$ mice at 8 weeks (Figures 1a and b) and also at 54 weeks (Supplementary Figure 1c).

Decreased HSC fraction in *Sf3b1*$^{+/-}$ mice

We evaluated HSCs and progenitor cells by flow cytometric analyses to further assess the hematopoietic system in the BM of 8-week-old mice. Interestingly, the frequency and the absolute number of HSCs, defined as CD34$^-$/low c-Kit$^+$ Sca1$^+$ Lineage$^-$ (CD34$^-$ KSL),[22] were significantly decreased in *Sf3b1*$^{+/-}$ mice (Figures 2a–c). On the other hand, there were no significant differences in the number of hematopoietic progenitor cell fraction (CD34$^+$ KSL cells), megakaryocyte–erythroid progenitors, common myeloid progenitors or granulocyte–monocyte progenitors between *Sf3b1*$^{+/+}$ and *Sf3b1*$^{+/-}$ mice (Figures 2a–f). *SF3B1* mutations were also seen in a subset of chronic lymphocytic leukemia cases, but no obvious changes in the common lymphoid progenitor population in BM were observed (Figures 2g–i).

Table 2. Bone marrow cell counts and spleen size of $Sf3b1^{+/+}$ and $Sf3b1^{+/-}$ mice at 8 weeks

Parameter	$Sf3b1^{+/+}$	$Sf3b1^{+/-}$	N	P-*value*
Total nucleated cells ($\times 10^7$)	5.04 ± 1.62	6.20 ± 0.84	6	0.15
Myeloid (%)	65.42 ± 4.35	66.67 ± 4.36	6	0.63
Erythroid (%)	17.08 ± 4.34	12.58 ± 3.43	6	0.07
Lymphoid (%)	13.58 ± 3.17	18.33 ± 5.17	6	0.08
Monocyte (%)	3.92 ± 2.85	2.42 ± 1.88	6	0.31
Megakaryocyte (6×10^4 nucleated cells)	7.00 ± 2.00	8.33 ± 1.75	6	0.27
Spleen weight (mg)	54.64 ± 9.83	64.64 ± 14.10	6	0.24

Data are the mean ± s.d. ($n = 6$).

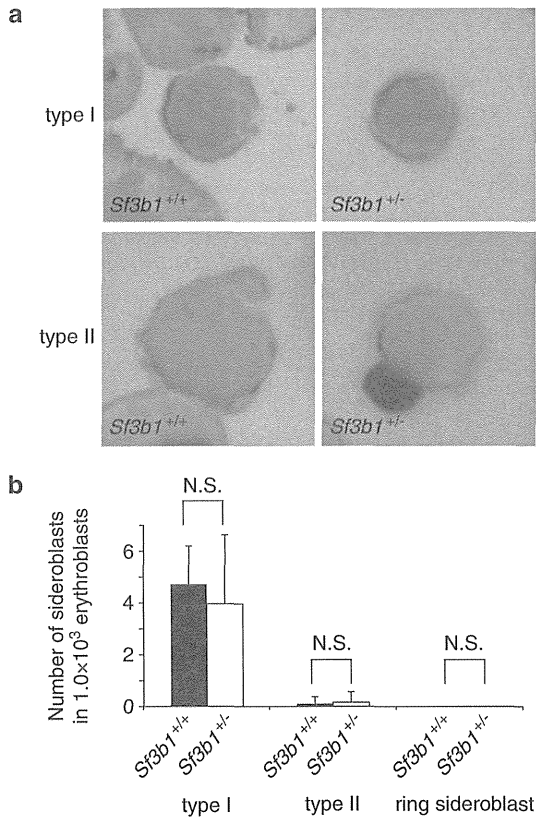

Figure 1. The number of sideroblasts is not increased in $Sf3b1^{+/-}$ mice. (**a**) Representative images of BM cytospin slides from $Sf3b1^{+/+}$ and $Sf3b1^{+/-}$ mice stained with Prussian Blue iron staining for the detection of sideroblasts. Sideroblasts were defined as follows: type I, sideroblasts with <5 siderotic granules in the cytoplasm; type II, sideroblasts with ⩾5 siderotic granules, but not in a perinuclear distribution; and ring sideroblasts with ⩾5 granules in a perinuclear position, surrounding the nucleus or encompassing at least one-third of the nuclear circumference. Original magnification × 1000. (**b**) The number of cells with siderotic granules counted per 1.0×10^3 erythroblasts; $n = 6$ mice per genotype. Data represent the mean ± s.d. NS, not significant.

In addition, splenic B cell populations were not significantly changed between $Sf3b1^{+/+}$ and $Sf3b1^{+/-}$ mice (Supplementary Figures 2a and b).

Next, we performed *in vitro* colony-forming cell assays using whole BM cells. Consistent with the reduction in the HSC fraction in $Sf3b1^{+/-}$ mice, the number of hematopoietic colonies in $Sf3b1^{+/-}$ mice BM cells was significantly lower than that in $Sf3b1^{+/+}$ mice (Figure 3a). No significant differences in the distribution of colony size or colony types were observed. These data also suggested that haploinsufficiency of *Sf3b1* leads to a decrease in the number of HSCs/immature progenitor cells, although there was no significant difference in the numbers of differentiated or mature blood cells.

Reduced number and impaired function of HSCs in $Sf3b1^{+/-}$ mice

Next, we assessed the reconstitution capacity of total BM cells from $Sf3b1^{+/-}$ mice using competitive repopulation assays. In these assays, 1.0×10^6 total BM cells from $Sf3b1^{+/+}$ or $Sf3b1^{+/-}$ mice ($CD45.1^-/CD45.2^+$) were transplanted into lethally irradiated recipient mice ($CD45.1^+/CD45.2^-$) with the same number of competitor cells from $CD45.1^+/CD45.2^+$ $Sf3b1^{+/+}$ mice. Then, the chimerism of donor-derived $CD45.1^-/CD45.2^+$ cells in the peripheral blood of recipient mice was measured by flow cytometry up to 40 weeks after transplantation. The chimerism of $Sf3b1^{+/-}$-derived $CD45.1^-/CD45.2^+$ cells in peripheral blood was significantly lower than that of $Sf3b1^{+/+}$ derived cells (Figure 3b), suggesting the compromised hematopoietic repopulation capacity of $Sf3b1^{+/-}$ mice. To confirm this finding further, we performed competitive repopulation assays using purified HSC fractions ($CD34^-$ KSL cells; Figure 3b). Similar to the result of competitive reconstitution assay using whole BM cells, the chimerism of donor-derived $CD45.2^+$ cells in peripheral blood was also reduced in the mice transplanted with $Sf3b1^{+/-}$ mice-derived HSCs compared with that in mice transplanted with $Sf3b1^{+/+}$ mice-derived HSCs. These observations suggested that the HSCs from $Sf3b1^{+/-}$ mice had significantly reduced reconstitution capacity compared with those from $Sf3b1^{+/+}$ mice (Figure 3b). The lineage contribution of $Sf3b1^{+/-}$ cells in peripheral blood was comparable with that of $Sf3b1^{+/+}$ cells (Figure 3b). These findings were confirmed by competitive repopulation assays using enriched long-term HSCs ($CD150^+$ $CD34^-$ KSL cells; Figure 3c).[23,24]

Furthermore, we performed serial transplantation experiments of whole BM and HSCs to assess the long-term reconstitution capacity of $Sf3b1^{+/-}$ HSCs more precisely. $Sf3b1^{+/-}$ mice showed reduced chimerism of donor-derived $CD45.2^+$ cells in the primary transplantations of competitive whole BM and competitive HSCs, and the reduced chimerism was even more pronounced after secondary transplantations (Figure 3d). In summary, HSCs in $Sf3b1^{+/-}$ mice reduce not only their number but also their competitive repopulation capacity of hematopoiesis.

The effect of *Sf3b1* haploinsufficiency on gene expression

To investigate the molecular mechanisms of the impaired function of HSCs induced by *Sf3b1* haploinsufficiency, we conducted gene expression analyses by RNA sequencing using $CD34^-$KSL cells isolated from $Sf3b1^{+/-}$ and $Sf3b1^{+/+}$ mice (Supplementary Table 3). Differentially expressed genes in $Sf3b1^{+/-}$ mice, including 1059 upregulated and 828 downregulated genes, from those of

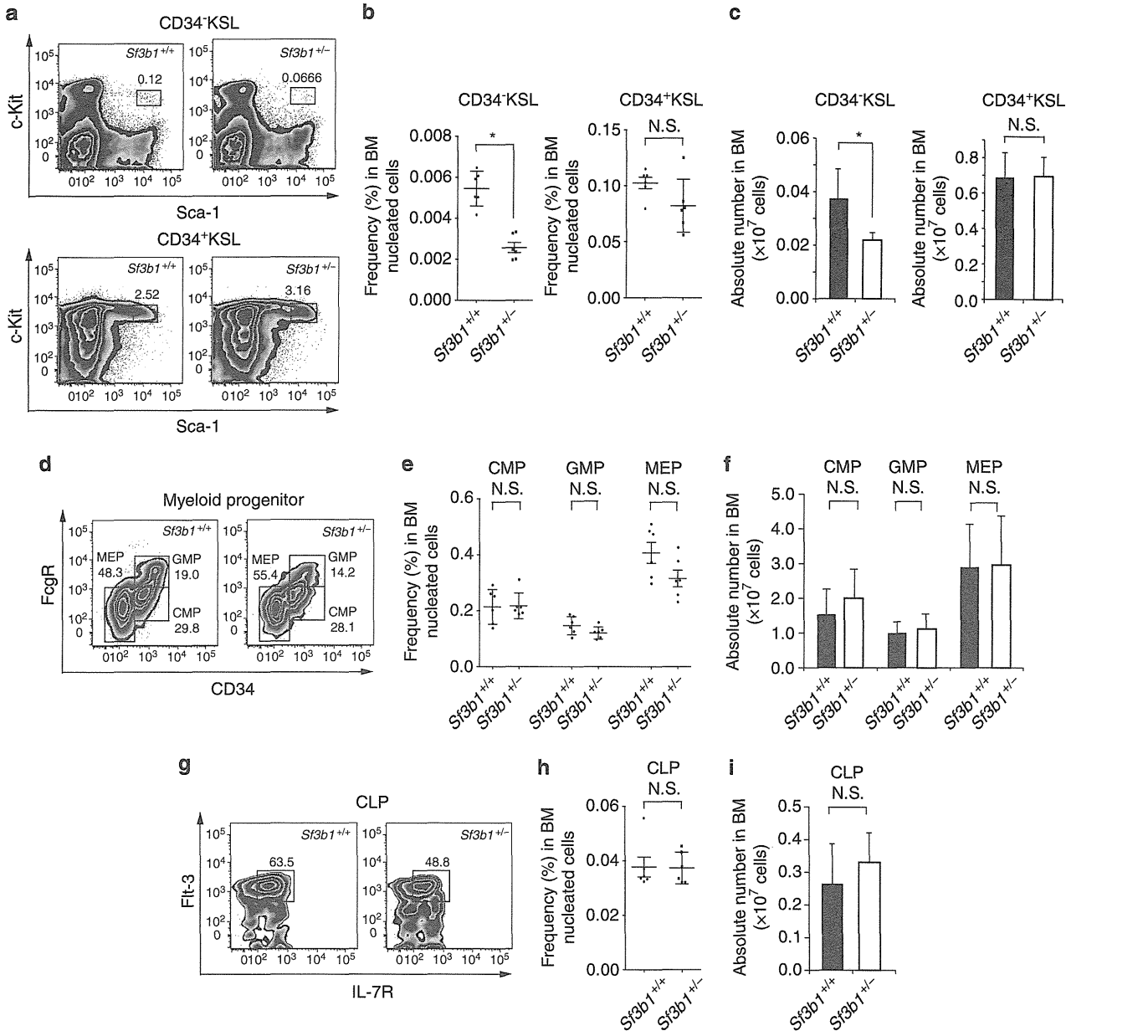

Figure 2. HSC population decreases in *Sf3b1*$^{+/-}$ mice. (**a**) Representative flow cytometric plot of HSCs (CD34$^-$KSL cells) and hematopoietic progenitor cells (HPCs; CD34$^+$KSL cells) from *Sf3b1*$^{+/+}$ and *Sf3b1*$^{+/-}$ mice. (**b**) Frequency of CD34$^-$KSL cells and CD34$^+$KSL cells in *Sf3b1*$^{+/+}$ and *Sf3b1*$^{+/-}$ mice BM. (**c**) Absolute number of CD34$^-$KSL cells and CD34$^+$KSL cells in *Sf3b1*$^{+/+}$ and *Sf3b1*$^{+/-}$ mice BM. (**d**) Representative flow cytometric plot of common myeloid progenitors (CMPs), granulocyte–monocyte progenitors (GMPs) and megakaryocyte–erythroid progenitors (MEPs) in *Sf3b1*$^{+/+}$ and *Sf3b1*$^{+/-}$ mice BM cells. CMPs are defined as Lin$^-$cKIT$^+$Sca1$^-$CD34$^{+/low}$FcgR^{int}, GMPs as Lin$^-$cKIT$^+$Sca1$^-$CD34$^+$FcgR$^+$ and MEPs as Lin$^-$cKIT$^+$Sca1$^-$CD34$^-$FcgR$^-$. (**e**) Frequency of CMPs, GMPs and MEPs in *Sf3b1*$^{+/+}$ and *Sf3b1*$^{+/-}$ mice BM. (**f**) Absolute number of CMPs, GMPs and MEPs in *Sf3b1*$^{+/+}$ and *Sf3b1*$^{+/-}$ mice BM. (**g**) Representative flow cytometric plot of common lymphoid progenitors (CLPs) in *Sf3b1*$^{+/+}$ and *Sf3b1*$^{+/-}$ mice BM cells. CLPs are defined as Lin$^-$ ckit^{low} Sca1^{low}IL7R$^+$Flt3$^+$. (**h**) Frequency of CLPs in *Sf3b1*$^{+/+}$ and *Sf3b1*$^{+/-}$ mice BM. (**i**) Absolute number of CLPs in *Sf3b1*$^{+/+}$ and *Sf3b1*$^{+/-}$ mice BM. Data are the mean ± s.d.; $n = 6$ per genotype. *$P < 0.05$. NS, not significant.

wild-type mice were detected (Supplementary Figure 3a and Supplementary Tables 4 and 5). Expression of *Sf3b1* in HSCs from *Sf3b1*$^{+/-}$ mice was reduced by ~45% compared with that in *Sf3b1*$^{+/+}$ HSCs, and this was confirmed by quantitative reverse transcriptase-PCR (Supplementary Figure 3b). Next, we performed the pathway analysis for differential expressed genes using GSEA, but GSEA identified no significant biological pathways, which explained the functional impairments in HSCs of *Sf3b1*$^{+/-}$ mice.

DISCUSSION

The *SF3B1* mutation is one of the most frequent genetic alterations in myelodysplasia and is also found in some chronic lymphocytic leukemia cases. Hence, the physiological role of *SF3B1* in the regulation of normal hematopoiesis provides an important clue to understand the role of *SF3B1* mutations in the pathogenesis of hematopoietic malignancies having the *SF3B1* mutation. Here, we showed

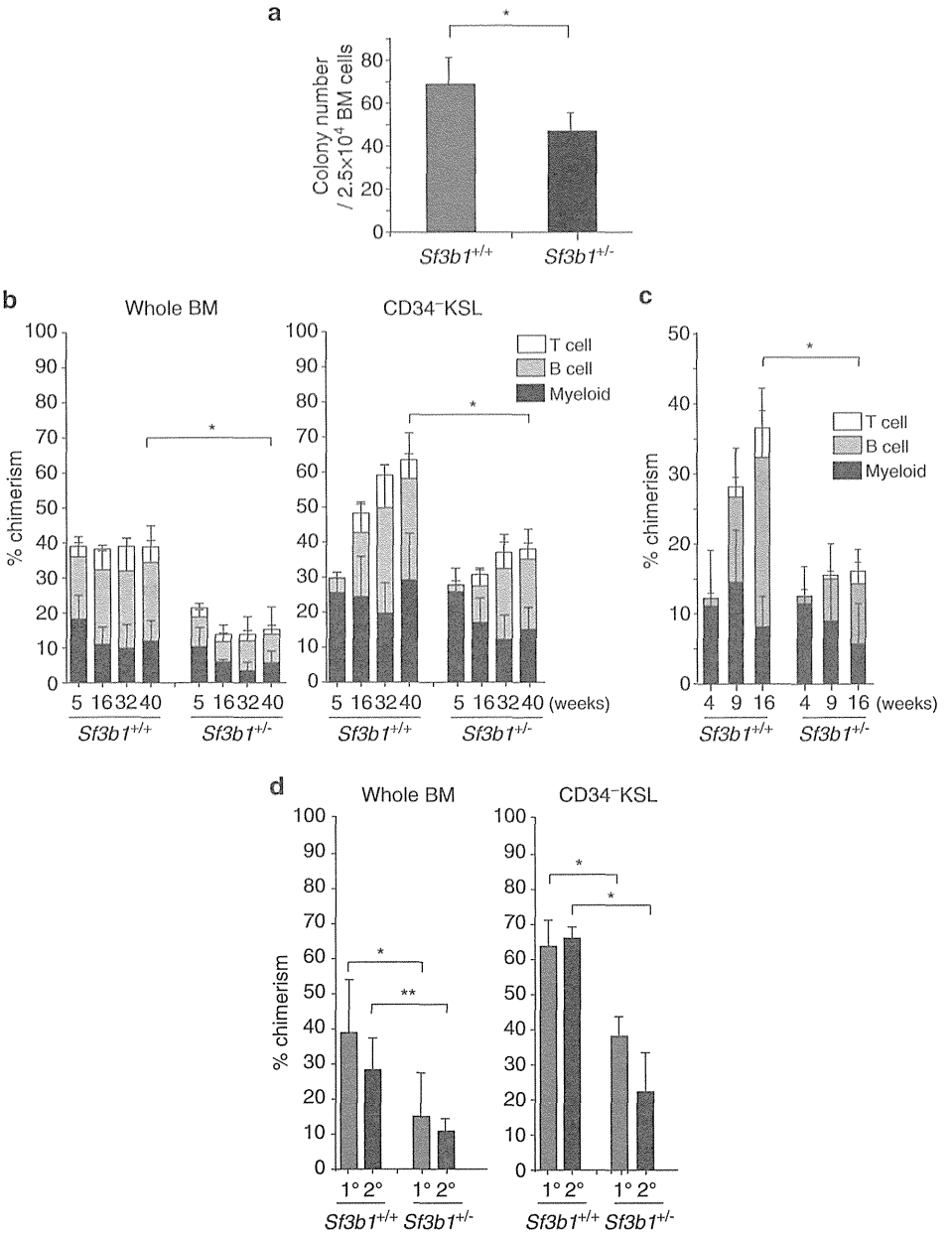

Figure 3. Reduced HSC numbers and impaired HSC function in *Sf3b1*$^{+/-}$ mice. (**a**) Total number of colony-forming units generated from whole BM cells. The number of colonies was counted after 14 days of culture. Data are the mean ± s.d.; $n = 4$ per genotype; $^{*}P < 0.05$. (**b**) Competitive transplantation using whole BM or HSCs; the vertical axis represents the average peripheral blood (PB) chimerism of donor-derived CD45.2^{+} cells. Data are the mean ± s.d.; $n = 13$ for whole BM transplantation, $n = 8$ for HSC transplantation; $^{*}P < 0.05$. (**c**) Competitive transplantation using enriched long-term HSCs (CD150^{+}CD34^{-}KSL cells); the vertical axis represents the average PB chimerism of donor-derived CD45.2^{+} cells. Data are shown as mean ± s.d.; $n = 5$, $^{*}P < 0.05$. (**d**) Serial transplantation assay; at 40 weeks post primary transplantation, BM cells harvested from the recipient mice were serially transplanted into additional secondary recipient mice. Chimerism of donor-derived CD45.2^{+} cells in peripheral blood at 40 weeks after primary transplantation (1°) and at 21 weeks after secondary transplantation (2°). Data are the mean ± s.d.; $n = 13$ for primary whole BM transplantation, $n = 8$ for primary HSC transplantation and $n = 5$ for both secondary transplantation per group; $^{*}P < 0.05$, $^{**}P < 0.01$.

unequivocally that *SF3B1* plays an important role in the regulation of HSCs.

In the present study, *Sf3b1*$^{+/-}$ mice showed a significantly reduced number of HSCs and compromised reconstitution capacity of hematopoiesis, although the underlying molecular mechanism remained elusive. SF3B1 is known as a core component of the mRNA splicing machinery, and therefore a possible mechanism would be altered RNA splicing caused by haploinsufficiency of the genes involved in stem cell regulation. Unfortunately, we failed to identify plausible genes whose splicing was specifically altered in *Sf3b1*$^{+/-}$ mice. The other possibility is that the mechanism is not related to RNA splicing. In fact, *Sf3b1*$^{+/-}$ mice have been reported to show posterior transformation of vertebrae, and this phenomenon was ascribed to deregulation of the expression of *Hox* genes without any accompanying defects in *Hox* gene splicing. The deregulated *Hox* gene expression is